

1
2 **SLUCM+BEM: A simple parameterisation for dynamic anthropogenic heat and**
3 **electricity consumption in WRF-Urban**
4

5 **Yuya Takane¹, Yukihiro Kikegawa², Ko Nakajima³, and Hiroyuki Kusaka⁴**

6 ¹ Environmental Management Research Institute, National Institute of Advanced Industrial Science
7 and Technology (AIST), Tsukuba, Ibaraki, Japan.

8 ² School of Science and Engineering, Meisei University, Hino, Tokyo, Japan.

9 ³ Renewable Energy Research Center, National Institute of Advanced Industrial Science and
10 Technology (AIST), Koriyama, Fukushima, Japan.

11 ⁴ Center for Computational Sciences, University of Tsukuba, Tsukuba, Ibaraki, Japan.
12

13 Corresponding author: Yuya Takane (takane.yuya@aist.go.jp)
14

15 **Key Points:**

- 16
- 17 • A new parameterisation for dynamic anthropogenic heat and electricity consumption is described.
 - 18 • The model reproduced the temporal variation and spatial distributions of electricity
19 consumption and temperature well in summer and winter.
 - 20 • The partial air conditioning was the most critical factor, significantly affecting the
21 value of anthropogenic heat emission.
- 22

23 **Abstract**

24 We propose a simple dynamic anthropogenic heat (Q_F) parameterisation for the Weather
25 Research and Forecasting (WRF)-single-layer urban canopy model (SLUCM). The SLUCM
26 is a remarkable physically based urban canopy model that is widely used worldwide.
27 However, a limitation of SLUCM is that it considers a statistically based diurnal pattern of Q_F .
28 Consequently, Q_F is not affected by outdoor temperature changes and the diurnal pattern of
29 Q_F is constant throughout the simulation period. To address these limitations, based on the
30 concept of a building energy model (BEM), which has been officially introduced in WRF, we
31 propose a parameterisation to dynamically and simply simulate Q_F from buildings (Q_{FB})
32 through physically based calculation of the indoor heat load and input parameters for BEM
33 and SLUCM. This method allows model users to simulate dynamic Q_F and electricity
34 consumption (EC) according to factors such as outdoor temperature changes, building
35 insulation, and heating and air conditioning (HAC) performance simply by setting the
36 AHOPTION option in URBPRAM.TBL to 2. SLUCM+BEM was shown to simulate

37 temporal variations of Q_{FB} and EC for HAC (EC_{HAC}) and broadly reproduce the EC_{HAC}
38 estimates of more sophisticated BEM and EC_{HAC} observations in the world's largest
39 metropolis, Tokyo. Our results demonstrate that SLUCM-BEM can be applied to urban
40 climates worldwide.

41 Plain Language Summary

42 In this study, we present a novel approach to improve the representation of
43 anthropogenic heat in urban areas within the widely used Weather Research and Forecasting
44 (WRF)-single-layer urban canopy model (SLUCM). The SLUCM is a well-established urban
45 canopy model, but has limitations such as assuming a statistically based diurnal pattern of
46 anthropogenic heat. To overcome these limitations, we incorporate a dynamic anthropogenic
47 heat parameterisation into SLUCM using the concept of a building energy model (BEM).
48 This new parameterisation allows for dynamic simulation of anthropogenic heat while
49 considering factors such as indoor heat load, building insulation, and heating and air
50 conditioning performance. By adjusting a specific setting (AHOPTION in URBPRAM.TBL),
51 users can easily simulate dynamic anthropogenic heat and electricity consumption in response
52 to external factors such as outdoor temperature changes. This improved model,
53 SLUCM+BEM, was able to reproduce anthropogenic heat estimates and observed electricity
54 consumption in Tokyo, the world's largest metropolis. SLUCM+BEM has the potential for
55 global application, providing a valuable tool for studying and understanding urban climates in
56 various regions worldwide.

57 1. Introduction

58 In the current era of climate change, cities are among the most critical sites for climate
59 change mitigation and adaptation. With urban development, population concentration and
60 urban warming, cities consume more energy and emit more greenhouse gases (GHGs) and
61 anthropogenic waste heat (Q_F) than ever. As a result, global and local urban warming will
62 continue to increase (IPCC 2021; Takane et al. 2019; 2020; Kikegawa et al. 2022). Against
63 this backdrop, climate change mitigation efforts toward the goal of carbon neutrality by 2050
64 are gaining momentum in countries across development stages, and urban climate change
65 adaptation efforts are also progressing. However, in countries and regions where urban areas
66 are expanding due to population and economic growth, GHG and Q_F emissions associated
67 with urbanisation are expected to continue to increase. In addition, energy consumption,
68 particularly for air conditioning (AC), is predicted to increase under continued global
69 warming in developed and other countries (IEA 2018). Therefore, clarifying the current state
70 of energy consumption, climate, and GHG emissions in urban areas and projecting these
71 factors into the future are essential strategies toward climate change mitigation and adaptation,
72 particularly for the development of a global climate change mitigation plan to achieve carbon
73 neutrality by 2050.

74 Urban canopy models (UCMs) represent a valuable method for physically estimating
75 and projecting urban warming, urban heat islands (UHI), and energy consumption (e.g.,
76 Kusaka et al. 2001; Chen et al. 2011). The UCM is an essential physical parameterisation for
77 the calculation of urban weather and climate, including the UHI effect. Several UCMs have
78 been developed by researchers worldwide and intercomparison experiments have been
79 conducted (Grimmond et al. 2010; 2011; Lipson et al. 2023). Among these models, some
80 UCMs have been officially implemented in the Weather Research and Forecasting (WRF)
81 model (Skamarock et al. 2021) and have many users worldwide (Chen et al. 2011). WRF
82 employs two main UCM options: the UCM alone, and a combined building energy model

83 (BEM). The UCM alone corresponds to the single-layer UCM (SLUCM, Kusaka et al. 2001;
 84 Kusaka and Kimura 2004), and a building effect parameterisation (BEP) (Martilli et al. 2002),
 85 whereas in the combined building energy model, the BEM is coupled to the BEP to construct
 86 BEP+BEM (Salamanca et al. 2010). Both UCM options have advantages and disadvantages.

87 The advantages of the SLUCM are that it requires fewer input parameters and has
 88 lower computational cost than the combined building energy model. However, in SLUCM,
 89 Q_F adopts a user-set diurnal pattern (Table 1). Thus, Q_F does not follow outdoor temperature
 90 changes, and the diurnal pattern of Q_F is constant throughout the simulation period.

91 By contrast, the advantages of the BEP+BEM model are that the heat emitted by
 92 buildings (Q_F from buildings [Q_{FB}]) varies with the outdoor temperature and human activity,
 93 allowing for dynamic calculation; and that electricity consumption (EC) associated with
 94 heating and AC (HAC) (i.e., EC_{HAC}) can be calculated (Table 1). However, the limitations of
 95 BEP+BEM are that Q_F from traffic is not considered, the BEM has numerous input
 96 parameters, and obtaining realistic parameter settings is difficult. Although calculations can
 97 be performed with default parameter inputs, the results of such calculations significantly
 98 overestimate measured EC when default parameters are entered (e.g., Takane et al. 2017; Xu
 99 et al. 2018). One suggested cause of this overestimation is that the setting (assuming an
 100 unrealistic situation) is based on the constant use of AC on all floors and in all buildings
 101 (Takane et al. 2017; Xu et al. 2018).

102 The aim of this study was to propose a new parameterisation, SLUCM+BEM, which
 103 exploits the advantages of both SLUCM and BEP+BEM, while compensating for the
 104 shortcomings of both models.

105

106 **Table 1** Description of urban canopy parameterisations.

	SLUCM ¹	SLUCM+BEM	BEP+BEM ²	CM-BEM ³	CLMU ⁴	BEM-TEB ⁵
Q_F from buildings	Prescribed	Dynamic	Dynamic	Dynamic	Dynamic	Dynamic
Q_F from traffic	Prescribed	Prescribed	–	Prescribed	Prescribed	Prescribed
Internal heat gains	–	Input	Input	Input	–	Input
EC_{HAC}	–	Dynamic	Dynamic	Dynamic	Dynamic	Dynamic
Partial AC	–	Implemented	–	Implemented	–	–
COP	–	Dynamic	Constant	Dynamic	Constant	Dynamic
Cooling tower	–	Implemented	–	Implemented	–	–
Windows	–	–	Implemented	Implemented	–	Implemented
Ventilations	–	–	Implemented	Implemented	Implemented	Implemented
Weekday–weekend difference	–	–	–	Implemented	–	–

107 AC, air conditioning; BEM, building energy model, BEP, building effect parameterisation; CLMU, community land model–
 108 urban; CM, canopy model; COP, coefficient of performance; EC, electricity consumption Q_F , anthropogenic heat, SLUCM,
 109 single-layer urban canopy model; TEB, town energy balance.

110 ¹ Kusaka et al. (2001), ² Salamanca et al. (2010), ³ Kikegawa et al. (2003), ⁴ Oleson and Feddema (2020), ⁵ Bueno et al.
 111 (2012)

112

113 The SLUCM+BEM proposed in this study has two main characteristics (Table 1).
 114 First, it resolves a limitation of SLUCM, the user-defined diurnal pattern of Q_F during the
 115 simulation/prediction period. Specifically, by introducing the BEM concept (Kikegawa et al.

116 2003; 2006; Salamance et al., 2010; Bueno et al. 2012; Oleson and Feddema 2020), heat
117 conduction through the wall and roof is calculated from the difference between the outdoor
118 air temperature and the building boundary temperature in the urban canopy space, and this
119 value and the indoor heat load are processed by HAC to calculate EC_{HAC} , thereby enabling
120 dynamic calculation of EC and Q_{FB} . As a result, improved accuracy can be expected on days
121 that deviate from the average conditions during the simulation period, such as hot or cold
122 days.

123 Second, SLUCM+BEM considers partial AC (in which AC is not used at all times, on
124 all floors, or in all buildings), coefficient of performance (COP) changes and cooling towers,
125 similar to CM-BEM (Kikegawa et al. 2003; Takane et al. 2022; Nakajima et al. 2023), which
126 is among the most detailed urban models incorporating a canopy model (CM) and BEM in
127 use today. Nevertheless, the parameterisation has been kept as simple as possible, e.g., by not
128 considering windows, which require uncertain parameter inputs. In this manner, the
129 advantages of BEP+BEM described above were exploited, and the corresponding
130 disadvantages were overcome.

131 As shown in Table 1, the SLUCM+BEM proposed in this study has similar
132 characteristics to CM-BEM. However, SLUCM+BEM is simpler than CM-BEM. A typical
133 simplification is the absence of windows in the buildings (such that the amount of solar
134 radiation entering the building is not considered in the calculation of the indoor heat load).
135 Although a previous study improved the SLUCM and introduced a detailed window sub-
136 model in their BEM-SLUCM, which is used only for offline simulations (Chen et al. 2021), it
137 should be noted that many offices and homes use window coverings during summer, and that
138 incoming solar radiation becomes small during winter. Moreover, this assumption has been
139 used in many similar models such as the community land model–urban (CLMU; Oleson et al.
140 2008, Oleson and Feddema 2020 and urban climate and energy model (UCLEM; Lipson et al.
141 2018). Furthermore, SLUCM+BEM is intended to be used in cities worldwide and a database
142 of global window areas does not yet exist. Therefore, these parameters cannot be set properly,
143 which may lead to results with large uncertainties. This shortcoming is unavoidable and
144 reasonable at present, as SLUCM+BEM is intended for use in cities worldwide.

145 During the development of SLUCM+BEM, emphasis was placed on minimising the
146 number of new parameters to be entered and simplifying its use compared to the original
147 SLUCM and BEP+BEM models, as well as on careful comparison of SLUCM+BEM with the
148 CM-BEM and observed data. Specifically, we designed SLUCM+BEM to be usable by WRF
149 users and original SLUCM users simply through changing the AHOPTION option in the
150 URBPRAM.TBL setting from 1 to 2.

151 There is significant importance in updating SLUCM, which has users worldwide, e.g.,
152 in Europe (Loridan et al., 2010; Tsiringakis et al., 2019), Asia (Miao et al. 2009; Takane and
153 Kusaka, 2011; Kusaka et al., 2012; 2014; Adachi et al. 2014; Doan et al., 2019), North
154 America (Georgescu et al., 2014; Krayenhoff et al., 2018), Oceania (Hirsch et al. 2021), and
155 South America (Umezaki et al., 2020) and is preferred by more than 90% of its users (NCAR
156 2015). A recent systematic review reported that WRF coupled with SLUCM is the most
157 commonly applied numerical tool for urban environmental studies at the city and regional
158 scales (Krayenhoff et al., 2021). In particular, the development of SLUCM+BEM will
159 improve the applicability of the WRF model by supporting the prediction and estimation of
160 EC and Q_{FB} emissions and will also drive shifts in the consumer sector toward carbon
161 neutrality. Furthermore, this improvement will be applicable not only to the Tokyo
162 metropolitan area, which is the target of this study, but to cities worldwide.

163 Notably, Q_{FB} and EC calculated in SLUCM+BEM are based on HAC use, which
164 seems appropriate given the rapid spread of HAC driven by climate change and economic
165 growth, and the background that heat pumps are positioned as renewable energy in the
166 European Union and are widely used for heating. The same assumption is used in BEP+BEM.
167

168 2. Methods

169 2.1 Model development

170 An overview of SLUCM+BEM is provided in Fig. 1. In conventional SLUCM, users
171 turn the consideration of sensible Q_F on or off by selecting 0 or 1 as the AHOPTION option
172 in the URBPRAM.TBL setting, respectively. For AHOPTION = 1, hourly values of sensible
173 Q_F , given as the product of its daily maximum (AH) and hourly variation factor
174 (AHDIUPRF), which are both prescribed in URBPRAM.TBL, are added to the sensible heat
175 flux Q_H calculated by SLUCM, thereby returning Q_F to the atmospheric first layer of the
176 WRF (Fig. 1a). Users also set the building indoor boundary conditions BOUNDR for roofs
177 and BOUNDNB for walls (hereafter referred to collectively as BOUND*) to 1 or 2, referred
178 to in Fig. 1 as “zero-flux” and “constant”, respectively. The default setting is BOUND* = 1
179 (i.e., zero-flux).

180 With BOUND* = 1 (i.e., zero-flux; Fig. 1a), the conductive heat fluxes through walls
181 and roofs at indoor boundaries are zero due to equilibrium between the indoor boundary
182 temperature (K) (TBLEND for walls and TRLEND for roofs) and the temperature (K) at the
183 fourth layer of walls and roofs (TBL(4) and TRL(4), respectively). Therefore, the simulation
184 assumes perfect insulation performance under this setting. With BOUND* = 2 (constant; Fig.
185 1b), the values of TBLEND are constant, allowing for imbalance with TBL(4) and thus
186 generating conductive heat fluxes at indoor boundaries. If the outdoor temperature in the
187 urban canopy space is higher than the value of TBLEND set in URBPRAM.TBL (often in
188 daytime during summer), conductive heat flux can penetrate indoors and then disappear from
189 the model, making buildings behave as heat sinks (i.e., the user-set Q_F assumes that such heat
190 can contribute to Q_F from air conditioners). By contrast, when the outdoor temperature is
191 lower than the value of TBLEND (often in winter), the opposite is true: the building becomes
192 a heat source (i.e., the building represents a heat-producing object in the urban canopy space).

193 At the core of the proposed SLUCM+BEM is a concept that solves the issue of energy
194 imbalance described above and obtains a more realistic energy budget for buildings under the
195 conditions of HAC by estimating the amount of heat sink or source that the buildings provide
196 under the conventional SLUCM setting of BOUND* = 2 (constant) and returning a part of
197 this heat to the urban canopy space. To achieve this aim, the model calculates conductive heat
198 fluxes through walls and roofs, estimates the indoor heat load and calculates Q_F and EC
199 associated with HAC (Fig. 1c). The addition of these newly calculated variables and newly
200 introduced parameters in SLUCM+BEM allows the model to conduct dynamic calculation of
201 Q_F and EC for each time and day.

202

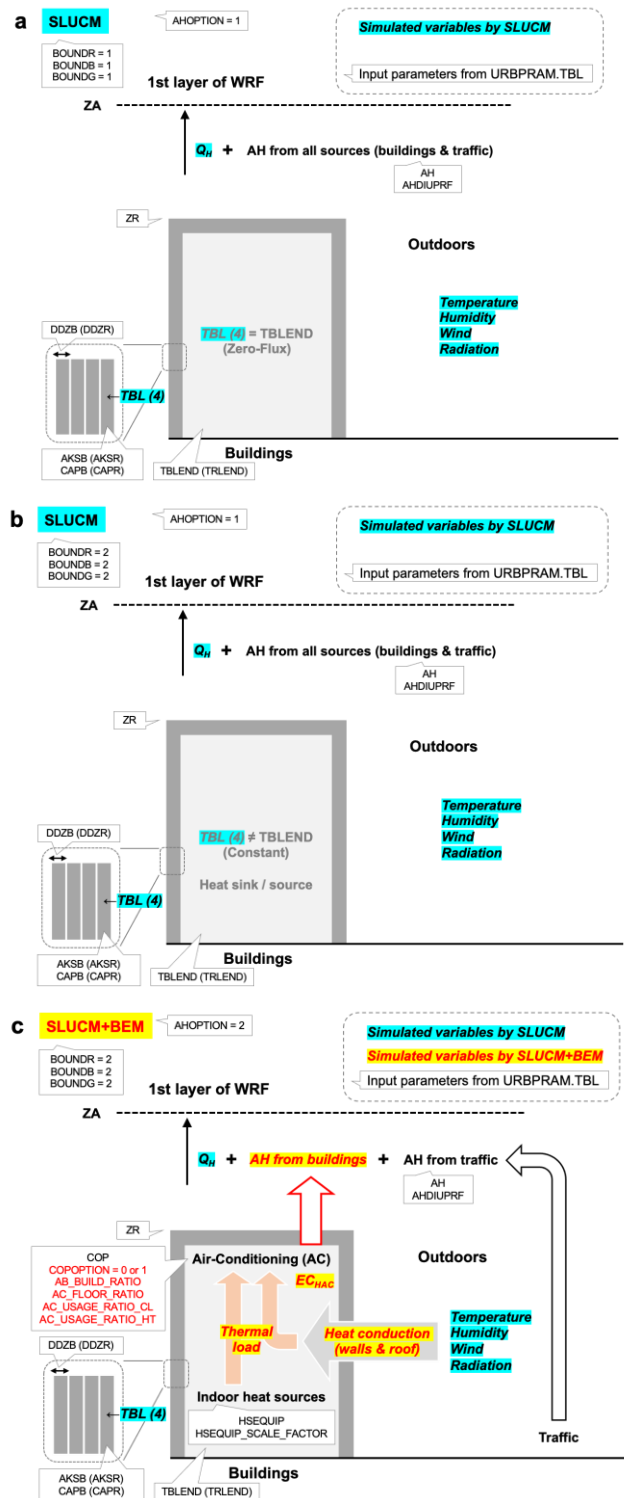


Figure 1 Schematic of energy budgets within the urban canopy layer including buildings, showing the single-layer urban canopy model (SLUCM) with the (a) “Zero-Flux” (BOUND* = 1) and (b) “Constant” (BOUND* = 2) settings, and (c) the updated SLUCM based on a building energy model (BEM), i.e., SLUCM+BEM, with the “Constant” setting. Blue and yellow highlighting indicate variables simulated by SLUCM and SLUCM+BEM, respectively. Text in callouts indicates original or newly introduced input parameters for URBPRAM.TBL in WRF.

203

204

Conductive heat transfer (HTRANS) is estimated as follows:

$$HTRANS = 2h AKSB \left(\frac{TBL(4) - TBLEND}{\left(\frac{DZB(4)}{2}\right)} \right) + r AKSR \left(\frac{TRL(4) - TRLEND}{\left(\frac{DZR(4)}{2}\right)} \right) \quad (1)$$

205 where the first and second terms on the right-hand side are conductive heat fluxes through
 206 walls and roofs, respectively; h and r are the normalised building height and roof width,
 207 respectively, as defined by Kusaka et al. (2001); $AKSB$ and $AKSR$ are the thermal
 208 conductivity of walls and roofs ($\text{W m}^{-1} \text{K}^{-1}$), corresponding to λ_W and λ_R in Kusaka et al.
 209 (2001), respectively; and DZB and DZR are the thickness of each layer of walls and roofs,
 210 respectively.

211 Following the estimation of $HTRANS$, indoor sensible heat load (H_{in} ; positive in
 212 summer and negative in winter) is calculated as follows:

$$H_{in} = HTRANS + A_f qE + A_f P \varphi_P q_{hs} \quad (2)$$

213 where the right-hand side shows each component of indoor sensible heat load. The first,
 214 second, and third terms indicate $HTRANS$ estimated with Eq. (1) (positive in summer and
 215 negative in winter), and internal sensible heat generation from the equipment and occupants,
 216 respectively (always positive). In addition, A_f is the floor area (m^2); qE is the sensible heat
 217 gain from appliances per floor area (W m^{-2}); P is the peak number of occupants per floor area
 218 (person m^{-2}); φ_P is the ratio of hourly occupants to P (dimensionless); and q_{hs} is the sensible
 219 heat generation from building occupants (W person^{-1}). For simplification, the model does not
 220 consider the transmission of solar insolation through windows or sensible heat exchange
 221 through ventilation.

222 Previous studies have reported that because BEP+BEM assumes central, rather than
 223 decentralised, HAC systems, BEP+BEM cannot distinguish between rooms with and without
 224 individual HAC units, leading to overestimations of EC_{HAC} (Takane et al. 2017; Xu et al.
 225 2018). Accordingly, HAC systems are assumed to operate in all buildings, floors, and rooms
 226 in BEP+BEM. This situation is not common in Asian cities, where mainly individual HAC
 227 units are used (e.g., Ihara et al., 2008; Kikegawa et al., 2014). Thus, to prevent overestimation
 228 of HAC use and improve the reproducibility of EC_{HAC} , we introduced the following three
 229 parameters, as described by Takane et al. (2017), considering the use of decentralised HAC
 230 systems: the ratio of abandoned houses/buildings to all houses/buildings (parameter a,
 231 AB_BUILD_RATIO), the ratio of air-conditioned floor area to total floor area (parameter b,
 232 AC_FLOOR_RATIO), and the ratio of electric HAC usage for cooling or heating to all
 233 cooling or heating equipment (parameter c, AC_USAGE_RATIO_CL and
 234 AC_USAGE_RATIO_HT for cooling and heating, respectively). Settings for these
 235 parameters are provided in Table 2. Regarding parameter a, many abandoned houses are
 236 present in Japan, which represents a social problem for the country. According to Osaka City
 237 (2015), the proportion of abandoned houses among the city's housing stock is 0.172, and it is
 238 reasonable to assume that these houses do not use HAC. For parameter b, the ratio of air-
 239 conditioned floor area to total floor area was reported by Kikegawa et al. (2014), with values
 240 of 0.71 and 0.05 in office and residential areas, respectively. Salamanca et al. (2013) also
 241 considered this ratio and demonstrated that BEP+BEM could reproduce the diurnal profile of
 242 electricity demand for AC when the value was set to 0.65 for the city of Phoenix, Arizona,
 243 USA. Regarding parameter c, most people use electric AC as cooling equipment during
 244 summer, whereas few people use electric AC systems as heat pumps during winter, as many
 245 other types of heating equipment are available. We used parameters a, b, and c to calculate
 246 the sensible heat load processed by HAC systems (H_{out} ; positive in summer, negative in
 247 winter) as follows:

$$H_{out} = H_{in} \times (1 - a) \times b \times c. \quad (3)$$

248 We calculated EC for HAC (EC_{HAC}) as follows:

$$EC_{HAC} = \frac{|H_{out}|}{COP}. \quad (4)$$

249 The coefficient of performance (COP) of the HAC system in Eq. (4) is realistically
250 reproduced by the following equation, after Kikegawa et al. (2005):

$$COP = \frac{rCOP \times fq \times z}{fp \times fx}, \quad (5)$$

251 where $rCOP$ is the nominal COP of the considered HAC system; fq and fp respectively
252 represent the dependency of the heating or cooling capacity and EC of the system on its
253 operational conditions as functions of the dry-bulb outdoor air temperature and the wet-bulb
254 indoor air temperature; z is the part-load ratio of the system; and fx represents the dependency
255 of fp on z . The functions fq , fp , and fx were taken from Kikegawa et al. (2005) for typical
256 Japanese HAC systems, as was $rCOP$.

257 Using H_{out} (Eq. 3), EC_{HAC} (Eq. 4), and COP (Eq. 5), the anthropogenic heat (Q_F) from
258 buildings (Q_{FB} ; positive in summer, negative in winter) was calculated at each time step as
259 follows:

$$Q_{FB} = H_{out} + EC_{HAC} = \frac{COP+1}{COP} H_{out} \quad ; \text{ during cooling operation (summer)} \quad (6)$$

$$Q_{FB} = H_{out} - EC_{HAC} = \frac{COP-1}{COP} H_{out} \quad ; \text{ during heating operation (winter)} \quad (7)$$

260 In the Northern Hemisphere, this study assumes the use of cooling during June–September
261 and the use of heating during November–March. In the Southern Hemisphere, the use of
262 cooling is assumed for November–March and the use of heating is assumed for June–
263 September. It is also possible to set the use of cooling and heating according to the outdoor
264 temperature calculated using SLUCM and WRF, rather than according to the month.

265 In business and commercial building (BC) grids, as described by Takane et al. (2017),
266 we divided Q_{FB} for cooling into sensible heat, $Q_{FB,S}$, and latent heat, $Q_{FB,L}$, referring to the
267 results of Shimoda et al. (2002) as follows, whereas all of Q_{FB} for heating was treated as
268 sensible heat:

$$Q_{FB,S} = 0.722Q_{FB} \quad (8)$$

$$Q_{FB,L} = 0.278Q_{FB}. \quad (9)$$

269 Shimoda et al. (2002) investigated the actual use of AC including electric and gas systems in
270 Osaka, and reported the ratio between $Q_{FB,S}$ and $Q_{FB,L}$ based on an inventory approach. $Q_{FB,L}$
271 was added to the latent heat flux, which is returned to the atmospheric first layer of the
272 meteorological and climate models.

273 2.2 Model settings

274 The present study used the Advanced Research WRF (ARW) ver. 4.3.2 (Skamarock et
275 al. 2021) and online coupling of WRF with SLUCM+BEM. Figure 2 shows the finest model
276 domain (d03), containing 251 grid points in the x and y directions, covering the Tokyo
277 Metropolitan Area (TMA), which was the focus of our study. Domains 1 (d01) and 2 (d02)
278 cover all of Japan and the central area of Japan, respectively. We set the horizontal grid
279 spacing to 25, 5, and 1 km for domains d01, d02 and d03, respectively. The model top was 50
280 hPa, with 37 vertical sigma levels. In this simulation, the initial and boundary conditions were
281 derived from the National Centres for Environmental Prediction Global Tropospheric Final
282 Analysis (NCEP–FNL) from the Global Data Assimilation System with 0.25° horizontal grid

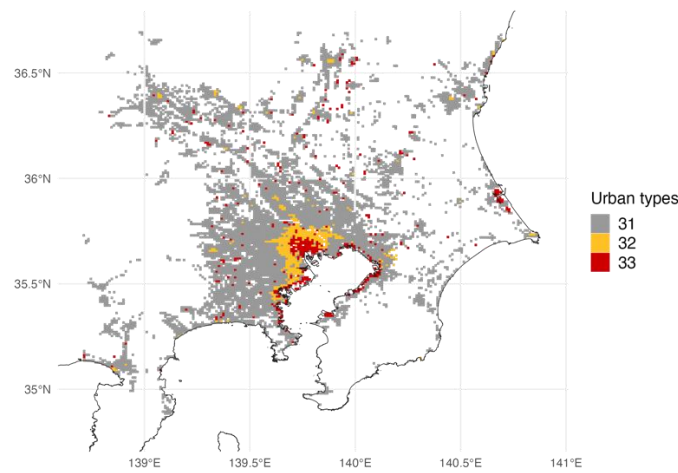
283 spacing (GDAS, 2015), and Group for High-Resolution Sea Surface Temperature (GHRSSST)
284 Level 4 data with 1-km horizontal grid spacing (Chao et al., 2009).

285 The following schemes were used in the simulation: updated Rapid Radiation Transfer
286 Model (RRTMG) short- and long-wave radiation schemes (Iacono et al., 2008), Morrison 2-
287 moment cloud microphysics scheme (Morrison et al., 2009), Mellor–Yamada–Janjic
288 atmospheric boundary-layer scheme (Mellor & Yamada, 1982; Janjic 1994; 2002), Noah land
289 surface model (Chen & Dudhia, 2001) and SLUCM (Kusaka et al. 2001; Kusaka & Kimura,
290 2004) or SLUCM+BEM as proposed in this study.

291 As in Takane et al. (2022) and Nakajima et al. (2021; 2023), building footprint
292 (polygon) data from a geographical information system in the TMA were used to identify
293 urban canopy geometry. The building use and total floor area for each building in the TMA
294 were recorded in the building footprint data. Land use–land cover (LULC) datasets produced
295 by the Geospatial Information Authority of Japan (GIAJ)
296 (<https://nlftp.mlit.go.jp/ksj/gml/datalist/KsjTmplt-L03-b-u.html>, last accessed 11/09/2023)
297 were used in this study. The urban grids were classified into three categories (C, Rm, and Rd)
298 based on the dominant building type, as shown in Figure 2a.

299

a



b



Figure 2 Study area. (a) Distribution of three building-use categories: residential area with detached

dwellings (low-density residential, 31 [grey]), residential area with multi-unit dwellings (high-density residential, 32 [yellow]), and business and commercial buildings (commercial, 33 [red]) in the Tokyo Metropolitan Area. (b) Terrain height within the study area. Open circles indicate observation sites at Nerima, Kumagaya, and Yoyogi, Tokyo.

300

301 We also used Automated Meteorological Data Acquisition System data for TMA
302 provided by the Japan Meteorological Agency as meteorological data for model validation.

303 The simulation was conducted from 09:00 JST (00:00 UTC = 09:00 JST) on 25 June
304 to 09:00 JST on 31 August 2018 for the summer case and 25 December 2016 to 28 February
305 2017 for the winter case. For each case, the first 5 days were discarded as the model spin-up
306 period.

307 We ran two simulation types: the original SLUCM with AHOPTION = 1 (BOUND* =
308 2; i.e., constant) and SLUCM+BEM with AHOPTION = 2 (BOUND* = 2; i.e., constant). The
309 main parameters entered for each simulation type are listed in Table 2.

310 In the SLUCM case, Q_F was an aggregate of all sources, with a maximum value (AH)
311 and temporal variation (AHDIUPRF) for each urban category. In this study, AH and
312 AHDIUPRF were obtained from the sum of Q_{FB} calculated by CM-BEM for each grid and
313 the separately input Q_F from traffic for each building category (Nakajima et al. 2023). In the
314 SLUCM+BEM case, Q_{FB} is the simulated variable, such that Q_F from traffic was given as AH,
315 and AHDIUPRF was the temporal pattern of Q_F from traffic, in accordance with Nakajima et
316 al. (2023). Notably, the ability to input Q_F from traffic in this manner is an advantage of
317 SLUCM+BEM over BEP+BEM (Table 1).

318 Both TRLEND and TBLEND are constant room temperatures, and their values are
319 based on realistic temperature settings for HAC in Tokyo (Takane et al. 2022; Kikegawa
320 2022; Nakajima et al. 2023). Different values were entered for summer and winter because
321 the temperature settings of HAC systems differ seasonally.

322 HSEQUIP_SCALE_FACTOR and HSEQUIP are the maximum value of the internal
323 heat gain and its percentage change over time, respectively. These parameters are used in both
324 BEP+BEM and SLUCM+BEM without alteration. The values were obtained from actual EC
325 data for the focal metropolitan area (Nakajima et al. 2023; Takane et al. 2023a).

326 AB_BUILD_RATIO is the ratio of abandoned houses/buildings to all
327 houses/buildings in a city block (parameter a in Eq. 3). This value can be set for each urban
328 category and was set to the value used by Takane et al. (2017).

329 AC_FLOOR_RATIO is the ratio of air-conditioned floor area to total floor area
330 (parameter b in Eq. 3). This value can be set for each urban category and was assigned the
331 temporally varying value for Tokyo adopted by Takane et al. (2022) and Nakajima et al.
332 (2023).

333 AC_USAGE_RATIO_CL and AC_USAGE_RATIO_HT are the ratios of electric
334 HAC use for cooling and heating to all cooling and heating equipment, respectively
335 (parameter c in Eq. 3). This value can be set for each urban category and was given the value
336 reported by Takane et al. (2017).

337 $rCOP$ in Eq. 5 is used in BEP+BEM to indicate the performance of HAC, and
338 SLUCM+BEM uses this parameter without alteration. Values from previous studies (Takane
339 et al. 2017; 2023; Kikegawa et al. 2022; Nakajima et al. 2023) were employed for $rCOP$.
340 Note that in BEP+BEM, COP is fixed at the input value of $rCOP$, whereas in SLUCM+BEM,

341 a formula was introduced to calculate realistic COP values (Eq. 5). However, COP can also
 342 be fixed at a constant value of $rCOP$ by setting $COPTION = 0$.

343 For both SLUCM and SLUCM+BEM, calculations are performed for two seasons,
 344 summer and winter; the TRLEND and TBLEND settings differ seasonally.

345

346 **Table 2** Parameter settings for the SLUCM and SLUCM+BEM models. The cooling and heating seasons
 347 (summer and winter) are defined as 25 June to 31 August 2018 and 25 December 2016 to 28 February
 348 2017, respectively. Urban categories are defined as 1 = low-density residential, 2 = high-density
 349 residential, and 3 = commercial.

Parameter (units) [cases]	SLUCM	SLUCM+BEM
Season	Cooling, heating	Cooling, heating
ZR (m) [Urban category = 1, 2, 3]	6.0, 10.0, 16.0	
FRC_URB (-) [Urban category = 1, 2, 3]	0.7, 0.9, 0.9	
AHOPTION (-)	1	2
AH ($W m^{-2}$) [Urban category = 1, 2, 3]	38.8, 52.8, 141.5 (from all sources, including buildings and traffic)	19.4, 26.4, 70.7 (from traffic only)
AHDIUPRF (-) [Local time = hours 1–24]	0.467 0.370 0.323 0.319 0.366 0.485 0.620 0.718 0.831 0.881 0.913 0.870 0.931 0.982 1.000 0.997 0.957 0.906 0.851 0.804 0.767 0.681 0.660 0.520	
BOUNDR, BOUNDNB, BOUNDG (BOUND*)	2	
DDZR (m) [Layer = 1, 2, 3, 4]	0.091, 0.091, 0.091, 0.091	
DDZB (m) [Layer = 1, 2, 3, 4]	0.093, 0.093, 0.093, 0.093	
CAPR ($J m^{-3} K^{-1}$) [Urban category = 1, 2, 3]	0.4521×10^6 , 1.588×10^6 , 1.298×10^6	
CAPB ($J m^{-3} K^{-1}$) [Urban category = 1, 2, 3]	0.674×10^6 , 1.702×10^6 , 1.598×10^6	
AKSR ($W m^{-1} K^{-1}$) [Urban category = 1, 2, 3]	0.071, 0.192, 0.094	
AKSB ($W m^{-1} K^{-1}$) [Urban category = 1, 2, 3]	0.094, 0.276 0.217,	
TRLEND (K) [Urban category = 1, 2, 3]	301, 301, 300 295.15, 295.15, 295.15	301, 301, 300 295.15, 295.15, 295.15
TBLEND (K) [Urban category = 1, 2, 3]	301, 301, 300 295.15, 295.15, 295.15	301, 301, 300 295.15, 295.15, 295.15
HSEQUIP_SCALE_FACTOR ($W floor-m^{-2}$) [Urban category = 1, 2, 3]	–	6.98, 8.42, 17.33
HSEQUIP (-) [Local time = hours 1–24]	–	0.67, 0.66, 0.65, 0.64, 0.64, 0.64, 0.68, 0.74, 0.83, 0.91, 0.96, 0.98, 0.99, 1.00, 0.99, 0.98, 0.99, 0.99, 0.95, 0.91, 0.86, 0.81, 0.77, 0.72
AB_BUILD_RATIO (-) [Urban category = 1, 2, 3] *	–	0.136, 0.136, 0.136
AC_FLOOR_RATIO (-) [Urban category =1, 2, 3], [Local time = hours 1–24] *	–	Urban category 1: 0.38, 0.35, 0.34, 0.32, 0.30, 0.28, 0.26, 0.23, 0.21, 0.17, 0.17, 0.17, 0.17, 0.16, 0.16, 0.16, 0.16, 0.18, 0.20, 0.23, 0.29, 0.34, 0.37, 0.40 Urban category 2: 0.45, 0.40, 0.35,

		0.33, 0.32, 0.31, 0.31, 0.31, 0.32, 0.33, 0.34, 0.34, 0.34, 0.34, 0.34, 0.34, 0.34, 0.35, 0.37, 0.39, 0.41, 0.42, 0.44, 0.45
		Urban category 3: 0.20, 0.19, 0.19, 0.18, 0.18, 0.18, 0.25, 0.37, 0.48, 0.56, 0.59, 0.62, 0.62, 0.62, 0.62, 0.62, 0.62, 0.62, 0.62, 0.55, 0.50, 0.44, 0.35, 0.24
AC_USAGE_RATIO_CL (-)	-	1, 1, 1
[Urban category = 1, 2, 3] *		
AC_USAGE_RATIO_HT (-)	-	0.6, 0.6, 0.6
[Urban category = 1, 2, 3] *		
COPTION (-) *	-	1
COP (-)	-	5.03, 5.03, 3.58
[Urban category = 1, 2, 3]		

350 AB_BUILD_RATIO, ratio of abandoned house/buildings to all houses/buildings in a city block;
351 AC_FLOOR_RATIO, ratio of air-conditioned floor area to total floor area; AC_USAGE_RATIO_CL,
352 ratio of AC usage for cooling equipment; AC_USAGE_RATIO_HT, ratio of AC usage for heating
353 equipment; AH, anthropogenic heat; AHDIUPRF, anthropogenic heating diurnal profile; AHOPTION,
354 anthropogenic heating option, where 0 = no anthropogenic heating, 1 = anthropogenic heating added to the
355 sensible heat flux term, 2 = anthropogenic heating from buildings simulated by SLUCM+BEM; AKSB,
356 thermal conductivity of the building wall; AKSR, thermal conductivity of the roof; CAPB, heat capacity of
357 the building wall; CAPR, heat capacity of the roof; COP, coefficient of performance; COPTION, switch
358 to determine whether COP is fixed or variable, where 0 = fixed COP, 1 = COP simulated by
359 SLUCM+BEM; DDZB, thickness of each building wall layer; DDZR, thickness of each roof layer;
360 FRC_URB, fraction of the urban landscape; HSEQUIP, proportional change of
361 HSEQUIP_SCALE_FACTOR over time; HSEQUIP_SCALE_FACTOR, peak internal heat gain;
362 TBLEND, lower boundary condition for building wall temperature; TRLEND, lower boundary condition
363 for roof temperature; ZR, building height.

364 * Newly added for SLUCM+BEM; (-) dimensionless parameter.

365

366 The SLUCM and SLUCM+BEM models were run in both offline and online modes,
367 coupled to WRF. In offline mode, Noah-LSM (Chen & Dudhia 2001) and SLUCM were
368 coupled with a mosaic of natural vegetation and urban tiles, in accordance with the online
369 WRF land surface processes. Meteorological data measured at a flux tower in Yoyogi, Tokyo
370 (Fig. 2b) (Hirano et al. 2015; Sugawara et al. 2021; Lipson et al. 2022) were used as forcing
371 data in offline simulations and the results were compared with the radiation budget and heat
372 fluxes measured at the same site. The settings for the online mode are described in Table 2.
373 The calculated online and offline temperature and electricity consumption were compared
374 with the corresponding measured values.

375

376 3. Results

377 3.1 Offline model verification

378 First, the offline versions of SLUCM and SLUCM+BEM were used to verify the
379 accuracy of reproductions of the summer radiation balance and surface heat budget observed
380 in Tokyo (Yoyogi, Fig. 2b) by Hirano et al. (2015), Sugawara et al. (2021), and Lipson et al.
381 (2022). Their results are shown in the upper part of Fig. 3; SLUCM and SLUCM+BEM
382 reproduced the radiation balance and heat budgets well (Fig. 3a, b). Focusing on the sensible
383 heat flux (Q_H), SLUCM somewhat overestimated the observations (Fig. 3a), whereas
384 SLUCM+BEM reproduced them well (Fig. 3b). In addition, SLUCM was unable to calculate

385 *EC* (Fig. 2a), whereas SLUCM+BEM both calculated *EC* and roughly reproduced the diurnal
 386 change of measured values in the Yoyogi area (Fig. 3b). The results of offline calculation
 387 with CM-BEM, a more sophisticated model, are shown in Fig. 3c. Both the radiation balance
 388 and surface heat budget were well reproduced, but Q_H was slightly out of phase, and
 389 SLUCM+BEM reproduced Q_H better than this result; for *EC*, CM-BEM reproduced the
 390 measurements very well, whereas SLUCM+BEM showed lower accuracy. Importantly,
 391 despite the modelling simplicity of SLUCM+BEM, it captured temporal changes to some
 392 extent.

393 The winter results were similar to the summer results: both SLUCM and
 394 SLUCM+BEM captured features of the radiation and surface heat budgets well (Fig. 3d, e);
 395 SLUCM+BEM did not capture diurnal changes in measured *EC*, but the daily averaged
 396 values generally aligned with observations (Fig. 3e). Notably, even the more sophisticated
 397 CM-BEM did not accurately reproduce temporal changes in winter *EC* (Fig. 3f). Therefore,
 398 difficulty in reproducing temporal changes in winter *EC* is not a drawback of SLUCM+BEM
 399 only.

400

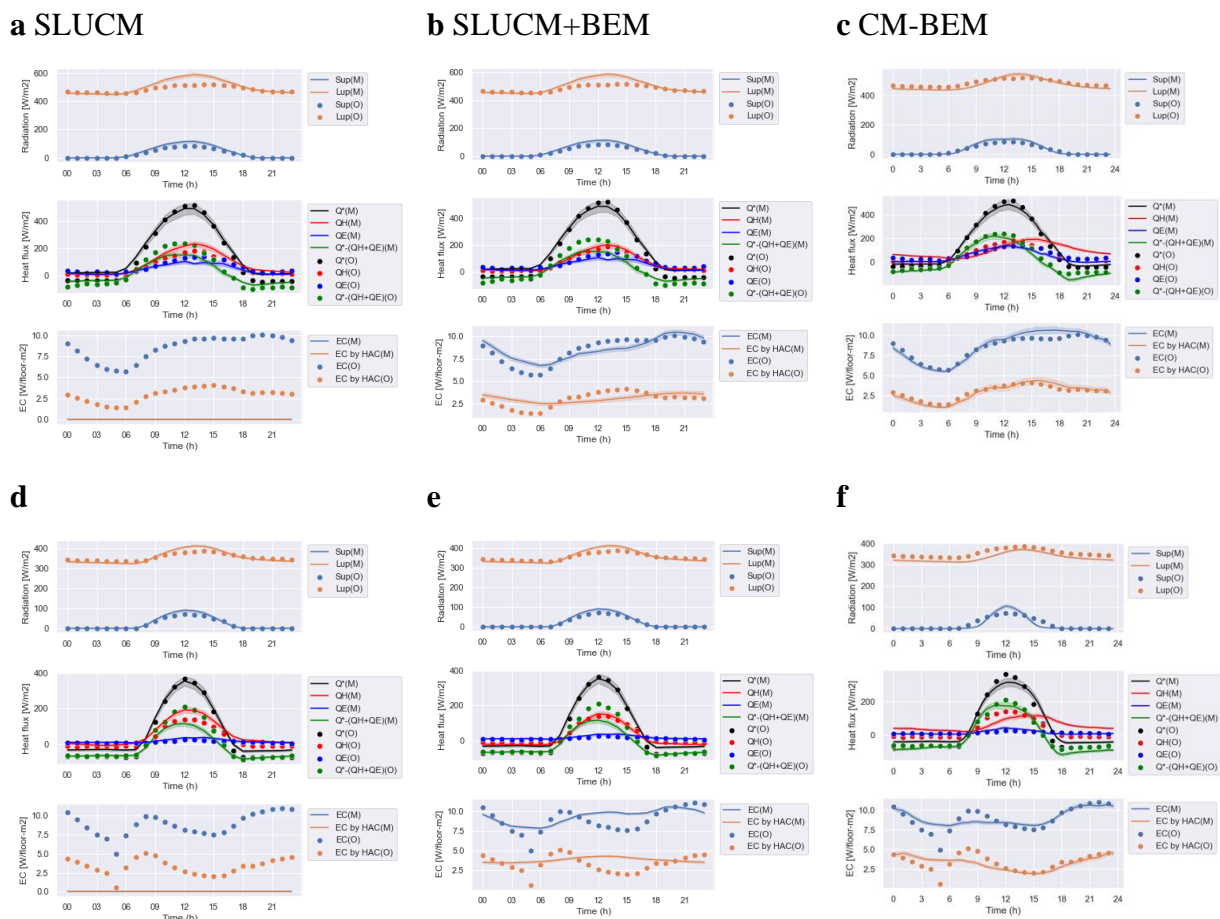


Figure 3 Diurnal changes in radiation, surface heat balance, and electricity consumption (*EC*) in Tokyo (Yoyogi [Fig. 2b]; Sugawara et al. 2021) averaged seasonally over (a–c) summer (July–August) and (d–f) winter (January–February). Circles are observations. Lines and error bars indicate simulated average values and standard deviations from (a, d) SLUCM, (b, e) SLUCM+BEM, and (c, f) CM-BEM, respectively.

401

402 3.2 Online model verification

403 3.2.1 Air temperature

404 This section describes the accuracy of reproducing temperatures calculated by the
405 online model (coupled version with WRF). Figure 4a shows the temporal variation of
406 temperature (monthly average by time of day) at three representative locations in the TMA by
407 building use: Tokyo (BC), Kumagaya (Rm), and Nerima (Rd) (Fig. 2b), where both SLUCM
408 (blue) and SLUCM+BEM (red) performed well in reproducing the observed temperatures
409 (black circles), with slightly better performance by SLUCM+BEM. For example, in Tokyo,
410 SLUCM had a mean absolute error (MAE) of 1.2°C, compared to 1.16°C for SLUCM+BEM,
411 and little difference between the two models at the other two sites. Both models reproduced
412 the horizontal temperature distribution in the metropolitan area better than its temporal
413 variation. For example, SLUCM+BEM reproduced the observed heat island centred on Tokyo
414 well (Fig. 5b) at 05:00 (Fig. 5a), and observed high temperatures in the inland area at 14:00
415 (Fig. 5d) were similarly well reproduced (Fig. 5c).

416 The winter results showed a similar trend to the summer results. Both SLUCM and
417 SLUCM+BEM captured characteristics of temporal temperature changes in Tokyo,
418 Kumagaya and Nerima well (Fig. 4b). However, both SLUCM and SLUCM+BEM showed
419 more significant errors for winter than for summer observations (Fig. 4a, b). The lower
420 accuracy of winter temperature reconstructions compared to summer is not limited to
421 SLUCM+BEM. For example, a similar trend was observed in the validation of BEP+BEM
422 (e.g., Takane et al. 2017). Gararro & González-Cruz (2023) also reported that the introduction
423 of electric heating reduced the peak UHI effect by 2.5–3°C. This temperature decrease during
424 winter is due to the negative Q_{FB} related to air-source heat pump AC systems used for heating.
425 For example, the MAE of SLUCM in Tokyo was 1.69°C, whereas that of SLUCM+BEM was
426 1.93°C. However, this error was strongly dependent on the input parameters, such as the AH
427 value input to SLUCM (Table 2). In general, it is not possible to precisely evaluate the
428 success of the two models comparatively, because in summer, both models reproduced the
429 horizontal distribution of temperature in the metropolitan area well, with SLUCM+BEM also
430 reproducing the observed heat island centred on Tokyo at 05:00 and the wider temperature
431 distribution at 14:00 (Fig. 5e–h).

432

433

434

435

436

437

438

439

440

441

442

443

444

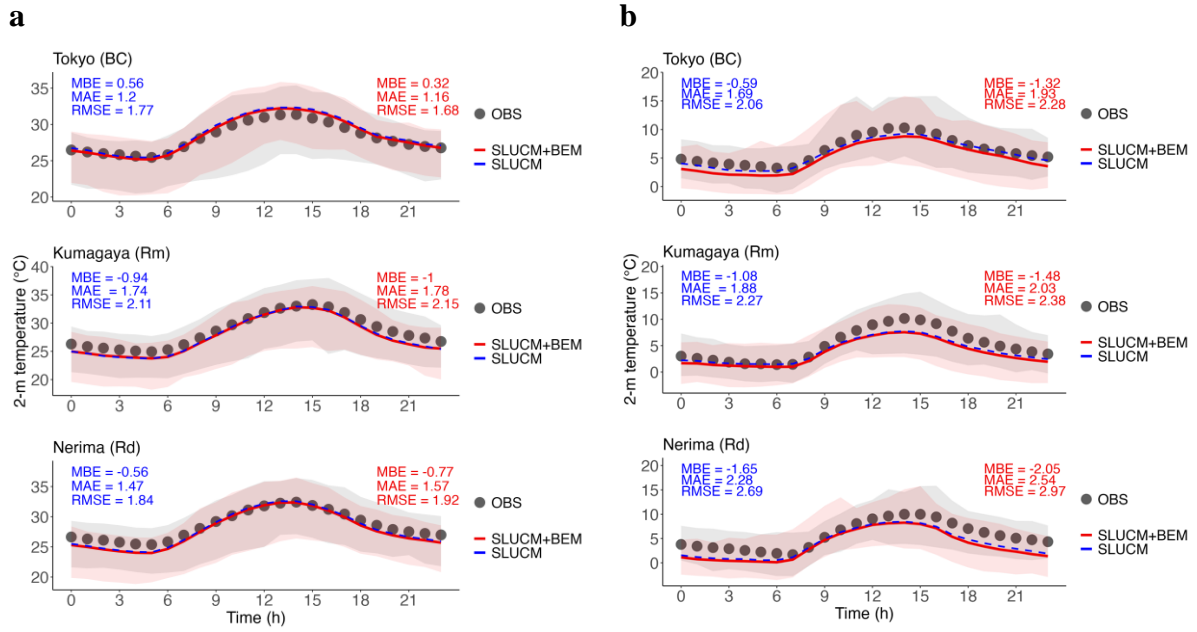
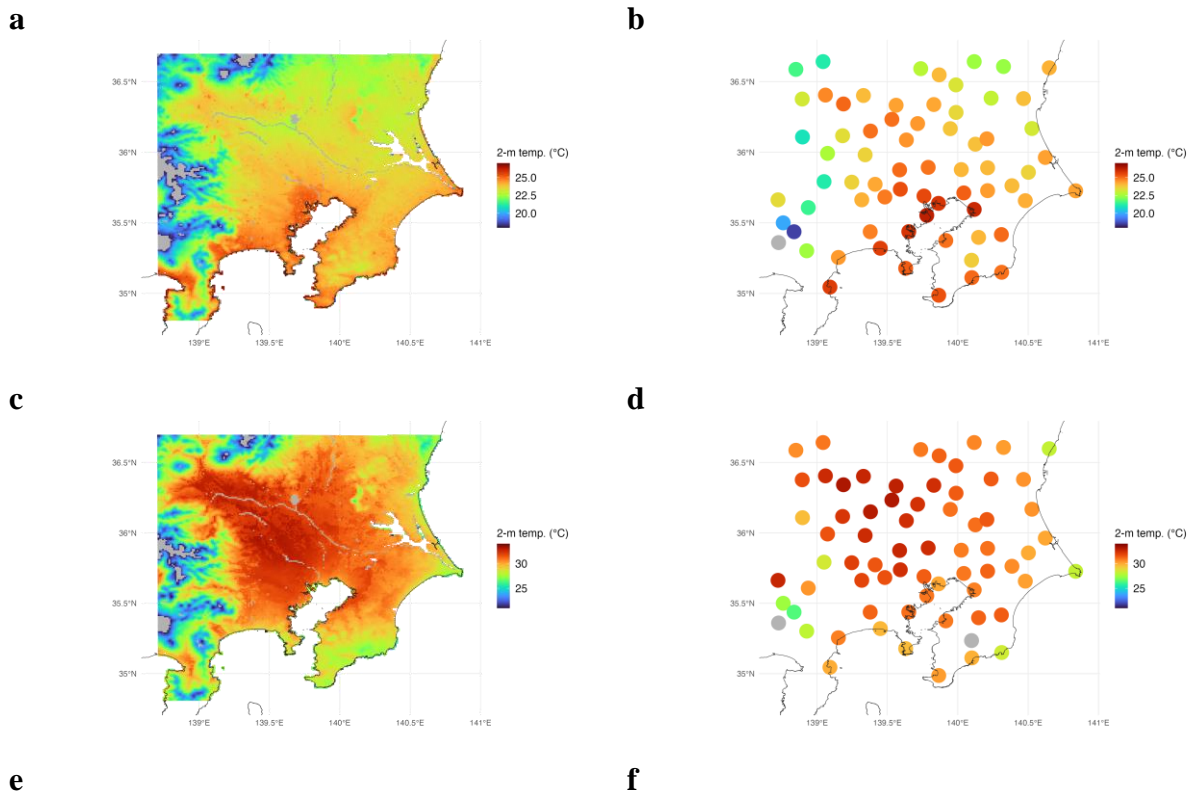


Figure 4 Diurnal changes in 2-m temperatures in Tokyo (BC), Kumagaya (Rm), and Nerima (Rd; Fig. 2b) averaged seasonally over (a) summer and (b) winter. Circles are observations. Lines and error bars are simulated average values and 5th-95th percentiles from SLUCM (blue) and SLUCM+BEM (red), respectively. MAE, mean absolute error; MBE, mean bias error; RMSE, root mean square error.

445



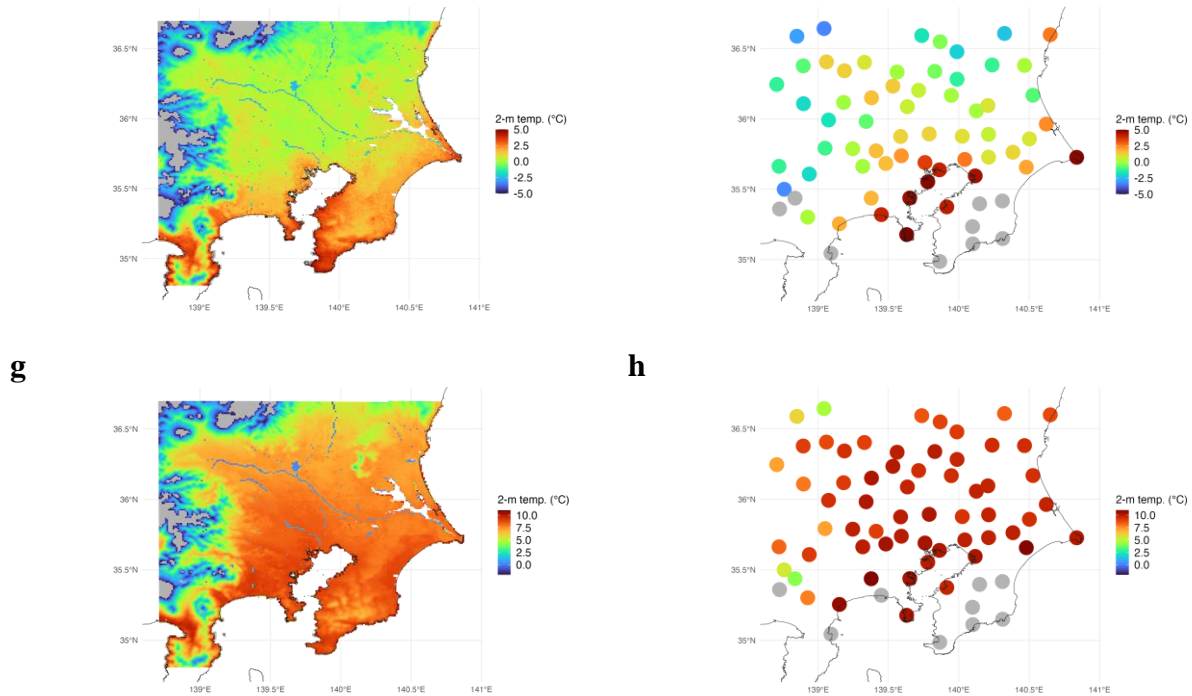


Figure 5 Distributions of observed (right) and simulated (left) 2-m temperatures in the Tokyo Metropolitan Area averaged for (a, b) 05:00 local time (LT) and (c, d) 14:00 LT in summer; and (e, f) 05:00 LT and (g, h) 14:00 LT in winter.

446

447 3.2.2 Electricity consumption (EC)

448 Notably, EC cannot be calculated with the existing SLUCM. Therefore, from this
 449 point on, we report the accuracy of EC reproduction only for SLUCM+BEM. In general,
 450 verifying the Q_{FB} for which SLUCM+BEM performs the simulation is difficult, because no
 451 method has been established for observing Q_{FB} . However, measured EC data are available. In
 452 this study, high-resolution EC observations for a metropolitan area reported by Nakajima et al.
 453 (2023) and Takane et al. (2023) are used to validate the accuracy of EC values calculated by
 454 SLUCM+BEM. In addition, we compare the validated results of SLUCM+BEM and CM-
 455 BEM. Note that if a model can reproduce EC , Q_{FB} can also be calculated realistically,
 456 according to Eqs. (4), (10), and (11).

457 We focused on the validation of EC_{HAC} , which is the variable simulated by the models.
 458 As observed EC_{HAC} , we used the EC_{HAC} estimated by Nakajima et al. (2022). One reason for
 459 validating EC_{HAC} rather than EC is that EC_{HAC} is the actual simulated variable, whereas EC
 460 includes input baseload parameters (HSEQUIP_SCALE_FACTOR and HSEQUIP). Thus, the
 461 validation result for EC contains errors both in simulated EC_{HAC} and in input parameters.
 462 Nakajima et al. (2022) showed that the baseload tends to vary even among BC grids of the
 463 same category in central Tokyo. CM-BEM can consider the variability of the baseload
 464 because it can input different baseload values in each model grid, but SLUCM+BEM uses
 465 only a single baseload value for each urban category (a uniform input across all BC grids;
 466 Table 2). Therefore, we focused on EC_{HAC} to compare only the simulated variable between
 467 SLUCM+BEM and CM-BEM.

468 Figure 6a provides a detailed map of EC_{HAC} in the Tokyo metropolitan area in summer
 469 (July–August 2018 average) as presented by Nakajima et al. (2023) and Takane et al. (2023).
 470 Figure 6b is a focused view of central Tokyo. EC_{HAC} is higher in the city centre and decreases
 471 toward the suburbs; SLUCM+BEM was generally able to capture this feature (city centre >

472 suburbs) (Fig. 6c, d vs. a, b). The errors of EC_{HAC} by building use and time within the area
473 shown in Fig. 6b, d are shown in Fig. 7 (upper). In Rm residential grids, the daily mean bias
474 error (MBE) was $1.5 \text{ W floor-m}^{-2}$ and $MAE = 1.7 \text{ W floor-m}^{-2}$. The Rd residential grids
475 produced slightly better results, with daily $MBE = 0.1 \text{ W floor-m}^{-2}$ and $MAE = 0.9 \text{ W floor-}$
476 m^{-2} . By contrast, BC showed daily $MBE = 4.4 \text{ W floor-m}^{-2}$ and $MAE = 4.9 \text{ W floor-m}^{-2}$,
477 indicating greater error than the residential results. EC_{HAC} tends to be high throughout the day.
478 Despite overestimation in the BC grids, the total error values for the area shown in Fig. 6b, d
479 were $MBE = 0.8 \text{ W floor-m}^{-2}$ and $MAE = 1.4 \text{ W floor-m}^{-2}$ for the daily average, because the
480 area of the BC grids was smaller than that of the Rm and Rd grids, as shown in Fig. 2.

481 For comparison with SLUCM+BEM, the results obtained from a more detailed model,
482 CM-BEM (Kikegawa et al. 2003; 2014; 2022; Takane et al. 2022; Nakajima et al. 2023), are
483 shown in Fig. 6e, f. The CM-BEM results cover a limited area due to the smaller
484 computational coverage of that model compared to SLUCM+BEM. Although the areas for
485 which the EC_{HAC} were calculated differ, the model resolution (1 km) and physical
486 parameterisations used are identical, except for the urban canopy and building energy model,
487 to allow for intercomparison. The CM-BEM results (Fig. 6f) reproduced the observations (Fig.
488 6b) well. In particular, SLUCM+BEM showed a relatively uniform EC_{HAC} for BC in the city
489 centre. In contrast, CM-BEM had different values in each grid, showing good agreement with
490 the observations. CM-BEM had lower error than SLUCM+BEM in BC, with daily $MBE =$
491 $1.9 \text{ W floor-m}^{-2}$ and $MAE = 2.3 \text{ W floor-m}^{-2}$. Possible reasons for CM-BEM outperforming
492 SLUCM+BEM in BC include the capacity of CM-BEM to consider differences in urban
493 morphology among grids and weekend conditions (lower EC_{HAC}) that differ from weekdays.
494 Thus, SLUCM+BEM uses the same urban morphology data for all BC grids and considers
495 only weekday conditions. In Rm residential grids, the daily mean error values were $MBE =$
496 $0.9 \text{ W floor-m}^{-2}$ and $MAE = 1.2 \text{ W floor-m}^{-2}$ (Fig. 7, bottom). As noted for the
497 SLUCM+BEM results, the Rd residential results were slightly better than the Rm residential
498 results, with daily mean error values of $MBE = 0.5 \text{ W floor-m}^{-2}$ and $MAE = 1.1 \text{ W floor-m}^{-2}$.
499 EC_{HAC} simulated by CM-BEM tended to be high only during daytime, in contrast to that
500 simulated by SLUCM+BEM. As shown in Fig. 6b, f, the daily average error values were
501 $MBE = 0.8 \text{ W floor-m}^{-2}$ and $MAE = 1.2 \text{ W floor-m}^{-2}$, which are similar to those of
502 SLUCM+BEM. Thus, although SLUCM+BEM is a simpler model than CM-BEM and can
503 cover a larger area, it performed as well as the detailed CM-BEM model in the detailed
504 validation of EC_{HAC} across the whole target area.

505 Note that the results presented above for CM-BEM are based on the latest version of
506 the code, which has been improved through grid-by-grid input of internal heat gain,
507 modelling of the AC operation schedule, and introduction of the proportion of AC systems in
508 BC grids. Based on these improvements, the errors were reduced (Nakajima et al. 2023).
509 These improvements provide clues for the future improvement of SLUCM+BEM.

510 The winter results were qualitatively similar to the summer results, but indicate
511 somewhat better performance of CM-BEM compared to SLUCM+BEM in the simulation of
512 EC_{HAC} . The distribution of winter EC_{HAC} and error estimates are presented in Figs. 8 and 9,
513 respectively.

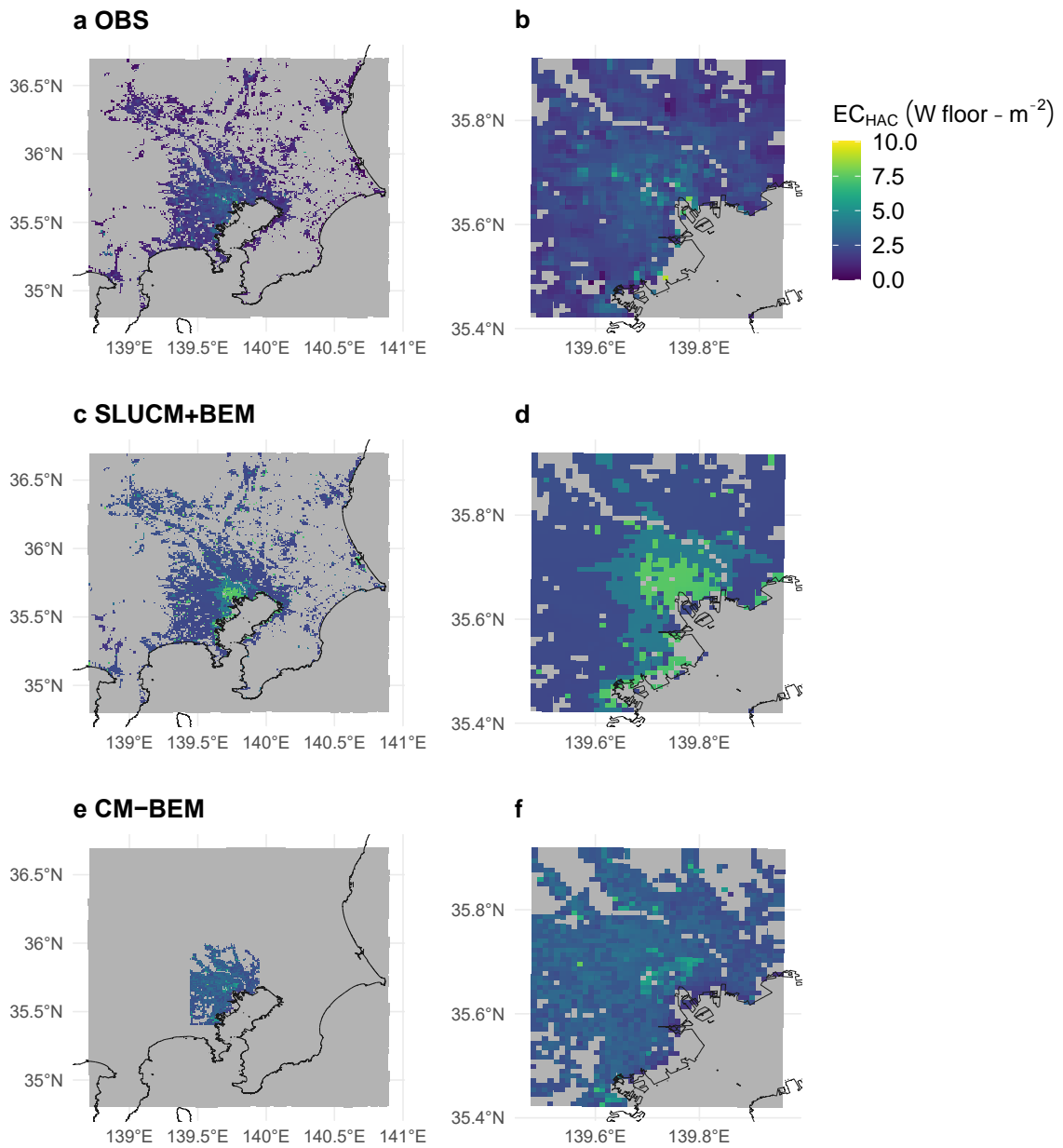


Figure 6 Distributions of (a, b) observed and (c–h) simulated electricity consumption (EC) for heating and air conditioning (HAC) (i.e., EC_{HAC}) in the Tokyo Metropolitan Area (left) and central Tokyo area (right) averaged over the summer season. Simulation results from (c, d) SLUCM+BEM, and (e, f) CM-BEM.

514

515

516

517

518

519

SLUCM+BEM

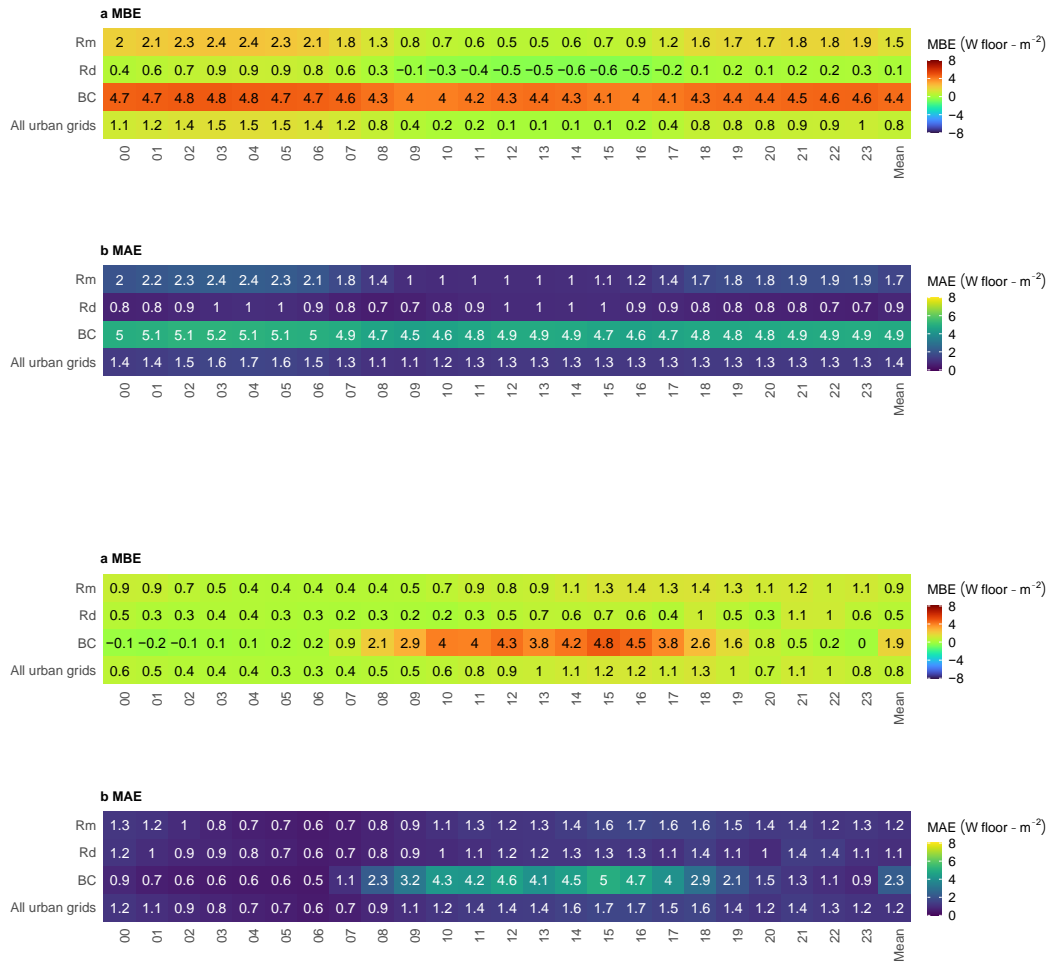


Figure 7 Diurnal changes in (a) MBE and (b) MAE of EC_{HAC} for each urban building use type, Rm, Rd, and BC, and the average of all grids from SLUCM+BEM (upper panels) and CM-BEM (new model; lower panels).

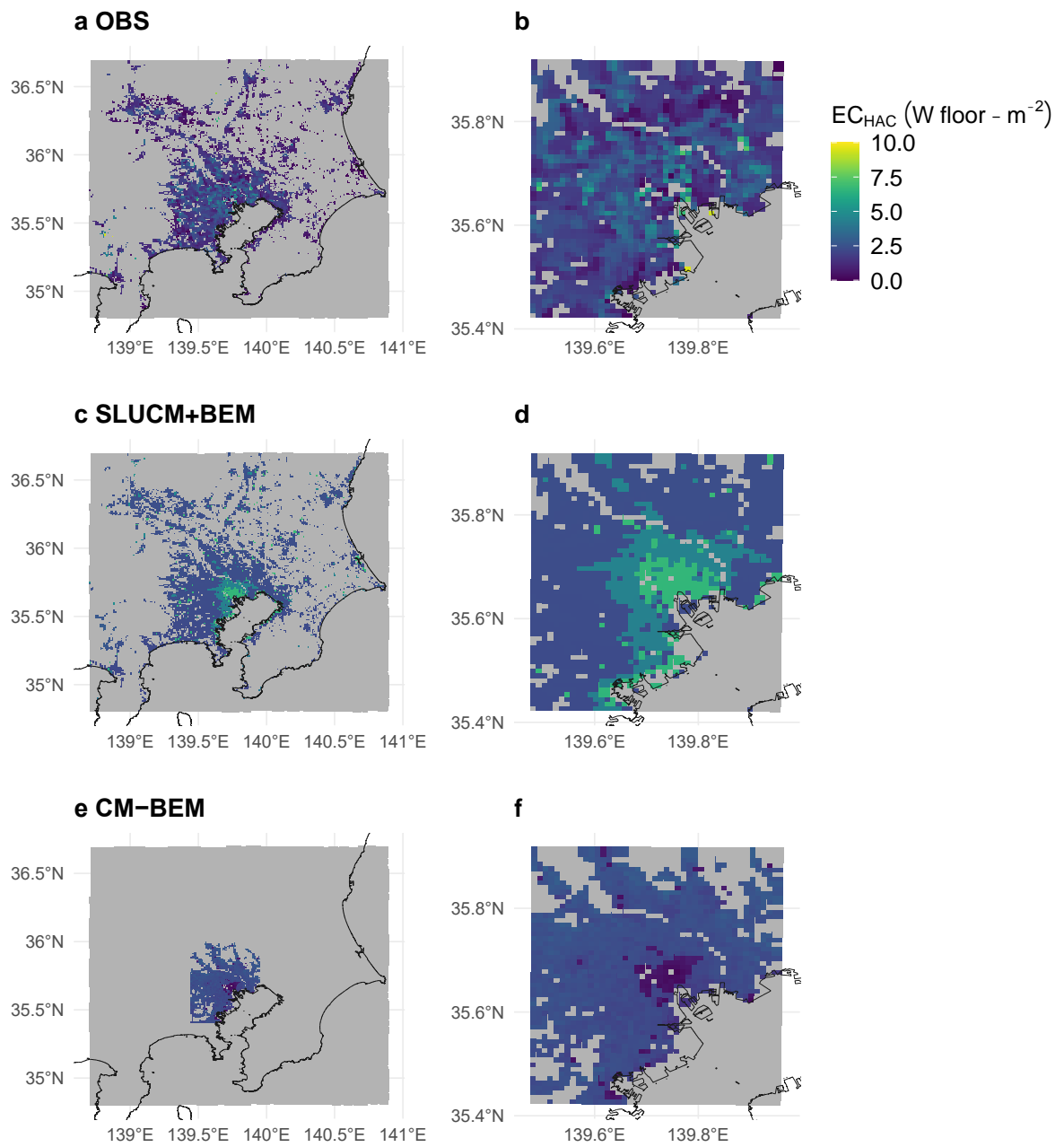


Figure 8 As described for **Fig. 6**, but showing results for the winter season.

521

522

523

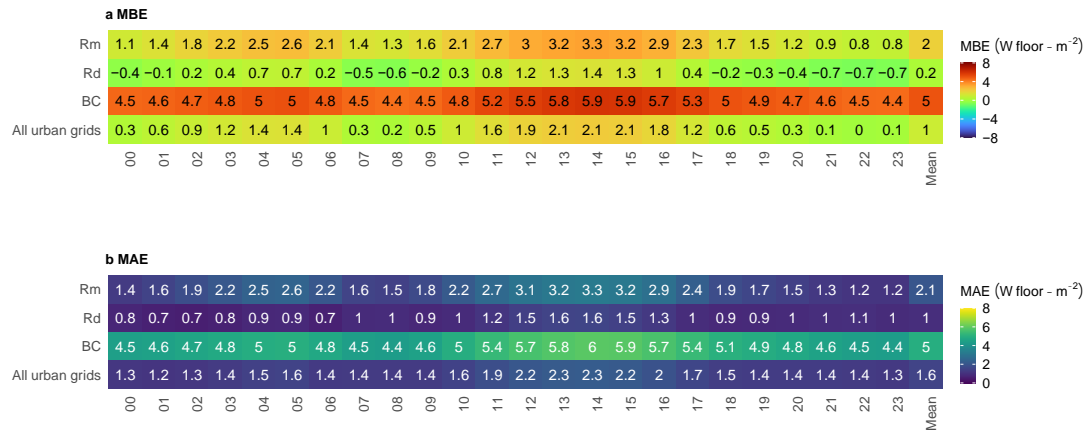
524

525

526

527

SLUCM+BEM



CM-BEM

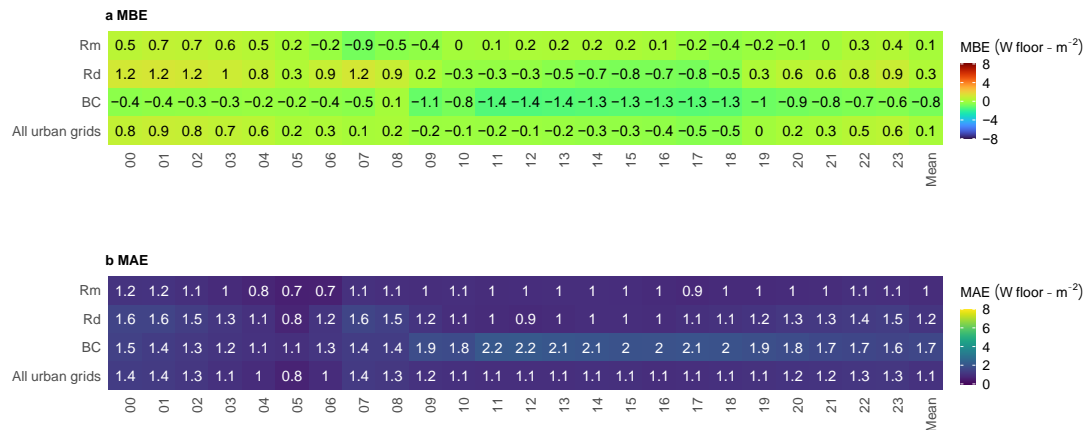


Figure 9 As described for **Fig. 7**, but showing results for the winter season.

528

529

3.2.3 Effects of temperature on EC and Q_{FB}

530

The EC_{HAC} calculation described above depends on the ambient temperature. The relationships between EC and air temperature at representative locations in Tokyo (BC), Kumagaya (Rm), and Nerima (Rd) are shown in **Fig. 10a**. In summer, EC and temperature were positively correlated; the slope of the regression line represents the temperature sensitivity of EC . Conversely, this correlation is negative in winter, with a smaller slope than in summer. One reason for the smaller slope in winter is that a lower proportion of buildings uses air conditioning for heating in winter than in summer (e.g., Takane et al. 2017).

537

Like EC , Q_{FB} can be calculated in a temperature-dependent manner (**Fig. 10b**). As also noted for EC , Q_{FB} and temperature are positively correlated in summer. In this case, winter also shows a positive correlation due to the use of air-source air conditioning is used, leading to heat absorption (i.e., negative heat is emitted) from the outdoor air during heating. This heat absorption is more significant at lower outdoor temperatures.

542

Notably, in the original SLUCM, EC is always zero, as it is not a target for calculation. The value of Q_{FB} does not respond to air temperature (see **Fig. 10**). By contrast, in

543

544 SLUCM+BEM, both EC and Q_{FB} can be calculated to respond to air temperature. It is a
 545 significant achievement that these two variables can now be calculated dynamically after
 546 addressing the shortcomings of SLUCM.
 547

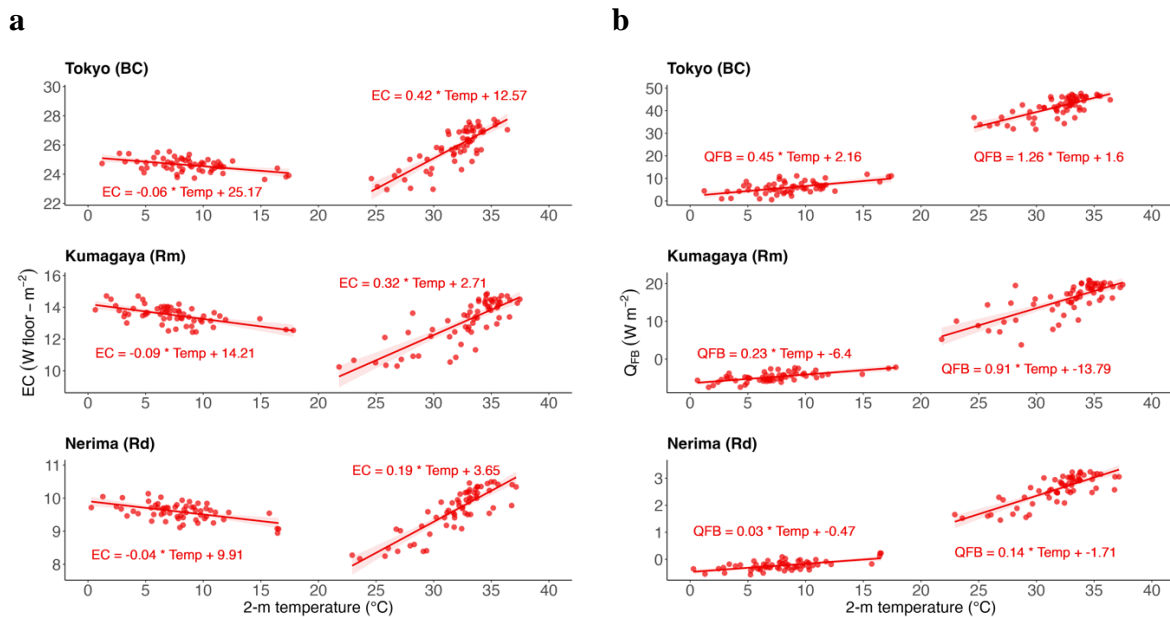


Figure 10 Scatterplots of 2-m temperature and (a) electricity consumption (EC), and (b) anthropogenic heat from buildings (Q_{FB}) in Tokyo (BC), Kumagaya (Rm), and Nerima (Rd) at 12:00 LT in summer and winter simulated by SLUCM+BEM. Each plot shows daily results. Lines with error bars are single regression lines. Plots with temperatures $> 20^\circ\text{C}$ represent calculation results for summer; those with temperatures $< 20^\circ\text{C}$ represent calculation results for winter.

548

549 4. Discussion

550 4.1 Importance of considering partial HAC

551 SLUCM+BEM includes features in the modelling of EC and Q_{FB} that are not
 552 considered in the BEP+BEM or officially included in the WRF, as follows.

- 553 • Consideration of partial HAC: BEP+BEM assumes that HAC is always in use on all
 554 floors and locations in the building, which is an unrealistic situation, and thus
 555 overestimates actual EC and consequently Q_{FB} emissions (Takane et al. 2017; Xu et al.
 556 2018). To avoid this overestimation, this study introduced the concept of partial HAC
 557 (Section 2.1) as described previously (Takane et al. 2017).
- 558 • Consideration of changes in COP: In BEP+BEM, COP has a fixed input value. In practice,
 559 COP generally varies with ambient temperature. The consideration of changes in COP
 560 allows more realistic dynamic calculation of EC and Q_{FB} .
- 561 • Consideration of the cooling tower: In BEP+BEM, all Q_{FB} is emitted as sensible heat,
 562 irrespective of building use. However, cooling towers exist in offices, and some Q_{FB} is
 563 discharged as latent heat during the cooling season, as demonstrated by the detailed
 564 cooling tower model in BEP+BEM (e.g., Yu et al. 2019) and in our separately developed
 565 CM-BEM. Therefore, in SLUCM+BEM, simplicity is emphasised, and fractions are
 566 introduced in Eqs. (7) and (8) to reproduce a simple cooling tower.

567 This section discusses how each of these features affects the Q_{FB} output. The results
568 for the control case, which considers all three of these items, are shown in Fig. 11a. Q_{FB} is
569 more significant in central Tokyo and more minor in the suburbs. The temporal variations at
570 three representative locations for each building use indicate that in Tokyo, Q_{FB} values
571 increase after 06:00 and reach 40 W m^{-2} at around 11:00, peak at around 18:00, and then
572 decrease. By contrast, in Kumagaya and Nerima, Q_{FB} values increase after 18:00, as more
573 people are present in their houses at night than during the day. Thus, residential areas use
574 more AC at night than during the day (Table 1, AC_FLOOR_RATIO). Although the value of
575 Q_{FB} is impossible to directly verify while considering all three of these factors, the calculation
576 is regarded as realistic because it reproduced EC well.

577 Figure 11b shows the results without the consideration of cooling towers. As cooling
578 towers are present only in offices, the results for residential areas are identical to those
579 obtained in the previous analyses. Focusing only on offices, the values for central Tokyo are
580 more significant than those shown in Fig. 11a. In terms of temporal variation in Tokyo, the
581 same Q_{FB} curve was obtained as described in the previous section, but the peak value during
582 the day was approximately 55 W m^{-2} , which is higher than the peak value of about 40 W m^{-2}
583 obtained in the control case (Fig. 11a). Thus, considering cooling towers led to an average
584 difference of approximately 15 W m^{-2} during the day.

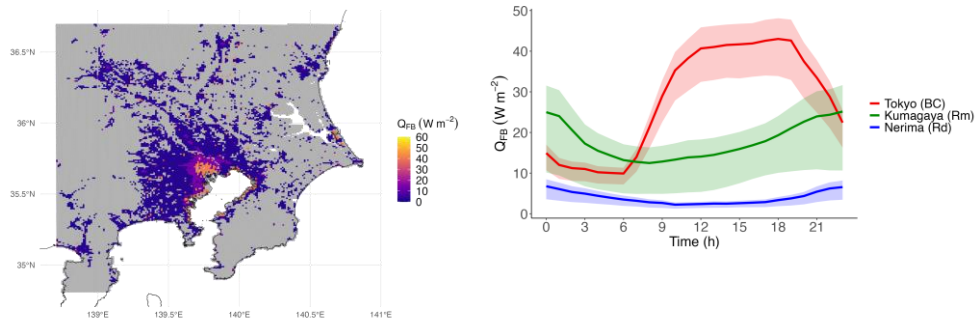
585 Next, we considered the effect of COP changes. Figure 11c shows the results
586 equivalent to Fig. 11b without considering COP changes, where COP is set to a fixed value.
587 These results demonstrate that the influence of COP changes was smaller than the change
588 illustrated in Fig. 11b; a comparison of Fig. 11b and c showed almost no change in the
589 mapping of Q_{FB} , and temporal changes were nearly identical at the three representative points.
590 However, the consideration of Q_{FB} changes is likely to be effective in heat wave analyses and
591 future projections of urban climate under the influence of global warming. Such calculations
592 involve significantly higher temperatures than those used in the present study, resulting in
593 lower COP and higher EC and Q_{FB} (Takane et al. 2019; 2020).

594 Finally, we considered the impact of partial HAC, changing the settings used in Fig.
595 11c to incorporate a whole-house HAC (similar to BEP+BEM). This case did not consider
596 partial HAC use. Comparing these results to the previous case, Q_{FB} for the whole
597 metropolitan area was more prominent with the whole-house HAC setting. Temporal changes
598 at three representative locations were also clearly affected. For example, in Tokyo, nighttime
599 Q_{FB} was greater for whole-house HAC than for partial HAC, and the difference between
600 daytime and nighttime values was smaller. Q_{FB} was approximately 100 W m^{-2} , regardless of
601 the time of day. Kumagaya showed no significant difference in the diurnal change pattern, but
602 the absolute values were consistently above 50 W m^{-2} . In Nerima, the pattern shifted to a
603 diurnal peak. Thus, the consideration of partial HAC critically impacted our results. To
604 include partial HAC in the model, new parameters such as those listed in Table 1 are needed
605 to accurately reflect the effects of human activity, slightly increasing the effort required for
606 analysis. However, the difference between Fig. 11c and d illustrates the benefit of considering
607 partial HAC whenever possible, as it has a strong impact on the results. In addition, we
608 recommend using social big data related to population, electricity, and HAC use, as real-time
609 population big data were used by Takane et al. (2022) to set these parameters.

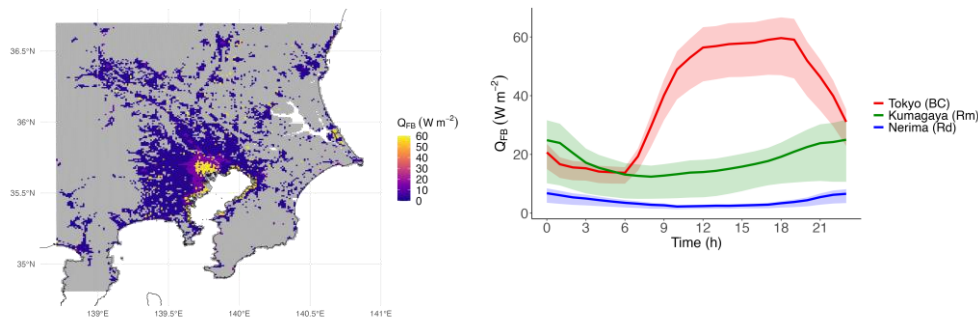
610 Overall, these results suggest that all three of the features included in SLUCM+BEM,
611 but not in BEP+BEM or WRF, for the modelling of EC and Q_{FB} should be considered. At a
612 minimum, partial AC should be considered.

613

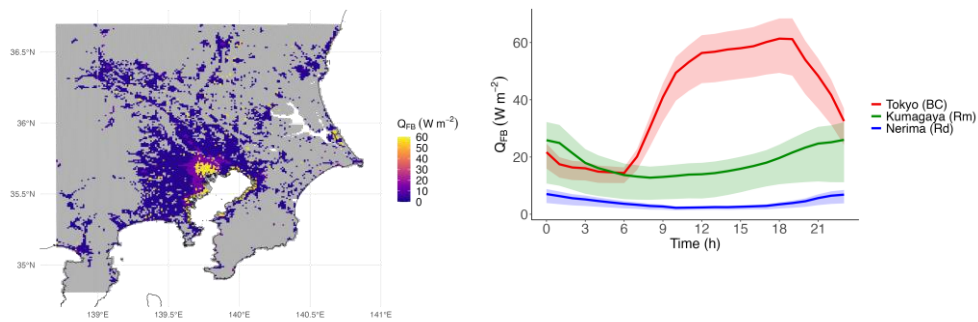
a CTRL



b No-cooling tower



c No-COP change



d No-partial HAC

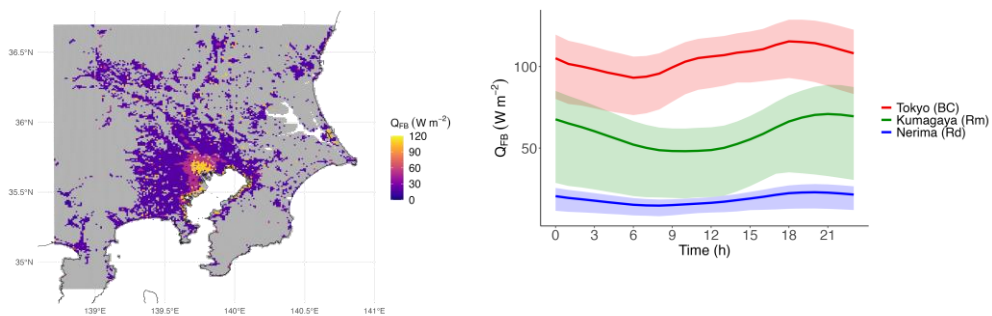


Figure 11 Distributions of simulated Q_{FB} in the Tokyo Metropolitan Area averaged for 14:00 LT in summer obtained from SLUCM+BEM (left). Diurnal changes in Q_{FB} in Tokyo (BC), Kumagaya (Rm), and Nerima (Rd) (right). Lines and error bars are simulated average values and 5th–95th percentiles, respectively. Simulation results are for cases including (a) control (CTRL), (b) no cooling towers, (c) no coefficient of performance (COP) change, and (d) no partial HAC.

615 4.2 Guidance for model selection

616 This section offers recommendations for model selection and the appropriate use of
617 three urban models, SLUCM, SLUCM+BEM, and CM-BEM, each of which has different
618 characteristics. An overview of the model selection process is provided in [Figure 12](#).

619 The most important difference affecting model selection is whether the user requires
620 dynamic calculation of Q_F and EC . If this calculation is not required, the original SLUCM is
621 suitable for use. Notably, the two approaches to improving this model differ depending on
622 whether BOUND* is set to 1 or 2 (see Sections 1 and 2.1). It is essential that Q_F (AH,
623 AHDIUPRF in URBPRAM.TBL) is entered as realistically as possible. If it is possible to
624 enter realistic values for Q_F obtained from energy consumption statistics compiled by the city
625 or country of interest or from existing global databases (e.g., [Varquez et al. 2021](#)), then it is
626 possible to reasonably simulate urban temperatures averaged over the simulation period (see
627 Sections 1 and 2.1). For example, when BOUND* = 1 (zero-flux), the building is assumed to
628 be perfectly insulated, whereas if Q_F is entered separately and includes realistic values for
629 heat removal from the building (Q_{FB}), then the calculation can be considered to reproduce
630 realistic conditions. Similarly, when BOUND* = 2 (constant), the building acts as a heat sink
631 or source at each time step, but if the energy lost or gained in this manner is added to Q_F in
632 advance, this calculation can also be considered to provide a realistic representation. In the
633 case of constant, we recommend that the boundary conditions TRLEND and TBLEND are
634 not set as the room temperature, but as the average outdoor temperature of the location during
635 the calculation period. The reason for this setting is that entering the average outdoor
636 temperature causes the calculation to assume that the energy balance between outdoors and
637 indoors is approximately balanced, at least when averaged over the calculation period. This
638 concept is similar to weather and climate simulations that use a bottom boundary condition of
639 land-surface models.

640 Users who have difficulty in setting realistic values for Q_F as described above, want to
641 calculate Q_F and EC dynamically, or want to simulate a period with high temperature
642 variations among days and time points are advised to use CM-BEM (or BEP+BEM as a
643 model of the same type) and SLUCM+BEM. However, these two models also have different
644 uses. Specifically, if Q_F and EC are required to be calculated in detail, such as considering a
645 building in multiple vertical layers and calculating the heat load of the building including
646 windows and ventilation, for realistic calculation of both EC and gas consumption, or if rich
647 input data related to these settings are available, then CM-BEM is an option.

648 If a single layer is sufficient instead of multi-layer analysis, if few input data are
649 available, or if there are concerns about the Q_F settings for SLUCM as described above, then
650 the SLUCM+BEM proposed in this paper is the optimal choice. Notably, SLUCM+BEM is a
651 parameterisation that assumes BOUND* =2 (i.e., constant) and the boundary conditions
652 TRLEND and TBLEND assume the temperature setting of the air conditioner (room
653 temperature), in contrast to the SLUCM constant setting.

654 As described above, SLUCM+BEM is a parameterisation that eliminates as many of
655 the shortcomings of both SLUCM and CM-BEM as possible, while incorporating as many of
656 their benefits as possible. According to [Chen et al. \(2021\)](#), inadequate representation of
657 building energy is included in many single-layer UCMs, including the surface urban energy
658 and water balance scheme (SUEWS) ([Järvi et al., 2011; 2014](#); [Ward et al., 2016](#); [Sun et al., 2024](#))
659 and the Arizona State University single-layer urban canopy model (ASLUM) ([Wang et al., 2013](#);
660 [Wang et al., 2021](#)). Our model, SLUCM+BEM, is the only model that couples a
661 single-layer UCM with BEM as well as WRF.

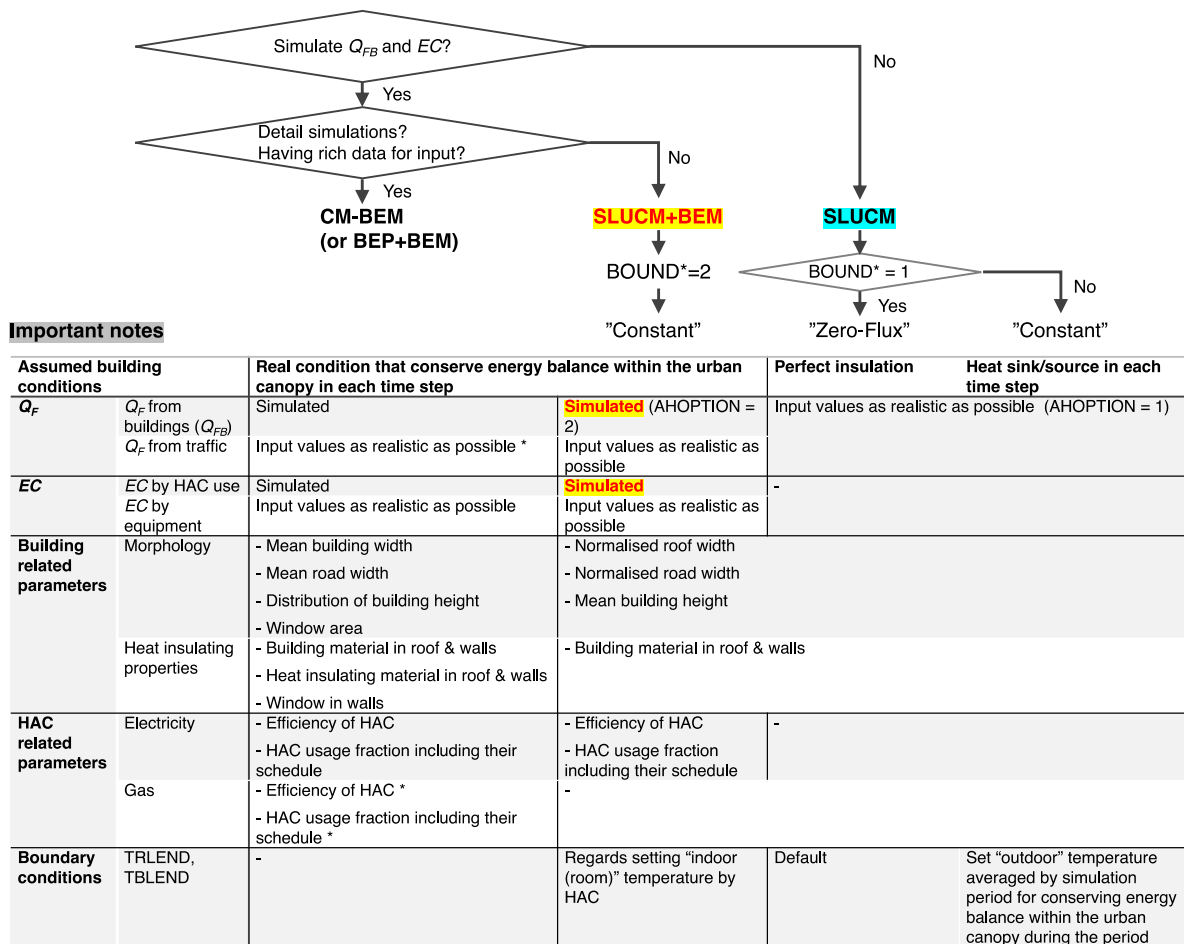


Figure 12 Flowchart of model selection process, highlighting important features and conditions of each model.

663

664 4.3 Limitations and future works

665 The factors that SLUCM+BEM ignores compared to the more detailed models
 666 BEP+BEM and CM-BEM are mainly windows and ventilation (Table 1). As no database of
 667 these factors exists at present, inaccurate window parameter inputs can lead to inaccurate
 668 calculation of indoor heat load, EC , and Q_{FB} . Therefore, we ignored these factors, because
 669 their inclusion deviates from the development policy of SLUCM+BEM, which was to
 670 develop the simplest model possible; we also ignored ventilation for the sake of simplicity.
 671 The extent to which these simplifications affect Q_{FB} and EC remains unclear. These
 672 improvements may be implemented in future research.

673 In addition, SLUCM+BEM considers only sensible heat. The balance of latent heat
 674 within and outside the building and the latent heat content of Q_{FB} are not calculated
 675 dynamically, in contrast to BEP+BEM and CM-BEM.

676 Furthermore, like BEP+BEM, SLUCM+BEM assumes weekday patterns for all
 677 calculations and does not consider weekends, whereas CM-BEM does differentiate weekends
 678 (Table 1). This change can lead to temperature differences of approximately 0.1–0.6°C in
 679 urban centres, particularly on holidays (Fujibe 1987; 2010; Bäumer & Vogel, 2007; Ohashi et
 680 al. 2016; Earl et al. 2016). This limitation may have led to an overestimation of EC_{HAC} in BC,

681 as described in Section 3.2.2. Nevertheless, the number of holidays is limited compared to
682 weekdays, and in this study, avoiding complexity was prioritised over this effect.

683 The most challenging point in parameterising Q_{FB} and EC is the treatment of heating.
684 In Japan, air-source heat pump AC units are also used for heating, but heating represents a
685 smaller percentage of their use than cooling (Takane et al. 2017; 2023). No accurate data on
686 the actual percentage of their service is available. Despite a trend toward using heat pump AC
687 units for heating in other countries, particularly in the EU, this practice is not yet common.
688 Therefore, winter calculations should be conducted with more caution than summer
689 calculations. We must emphasise that the same limitation and caution must be applied for
690 existing models such as BEP+BEM. In addition, this parameterisation based on air-source
691 heat pump AC will become increasingly useful in future scenarios, given that heat pumps are
692 positioned as a renewable energy source, are currently attracting attention, and will be widely
693 used in the future for the sake of energy security. By contrast, CM-BEM considers heating
694 types other than air-source heat pump AC (e.g., Kikegawa et al., 2003). Nonetheless, this
695 CM-BEM setting is too complex for meteorologists and climatologists, who are the main
696 users of WRF, and the data on which this setting is based are not standard. SLUCM+BEM
697 avoids this complexity.

698 The BEM developed in this study shares certain challenges with other BEMs.
699 Although the BEM can accurately calculate the temporal variation and spatial distribution of
700 anthropogenic heat emissions, it may not correctly calculate their long-term average values
701 and spatial averages. This issue is reminiscent of the shortcomings of the bottom-up approach
702 used to create anthropogenic heat emission databases from statistical data for energy
703 consumption amounts. When creating anthropogenic heat emission databases, this problem
704 could be addressed by concurrently employing a top-down approach, in which anthropogenic
705 heat emission data are calculated based on a statistical energy consumption database. Users of
706 the BEM may address this issue by skilfully adjusting parameters while verifying the
707 estimated anthropogenic heat against statistical data.

708 In general, if the information input to the model (optimal input data, parameter
709 settings) is insufficient, a more sophisticated model will have worse accuracy. In other words,
710 there is an inextricable link between the information input to the model and the accuracy of
711 the simulation results (e.g., Takane et al. 2023b). Therefore, users should carefully consider
712 the information available for their target city and select a model that is appropriate for that
713 information. In addition, the most important method for improving the accuracy of the model
714 may be the development of urban information, including morphological parameters (e.g.,
715 Khanh et al. 2023) and social big data such as real-time population and energy consumption
716 data (e.g., Takane et al. 2023b), which can effectively exploit the potential of a sophisticated
717 model such as BEM.

718 Future studies will include the projection of Q_{FB} emissions, EC , and urban climates
719 under future climate conditions, direct comparison with BEP+BEM, addressing the local
720 climate zone (Demuzere et al., 2022), and application to cities other than Tokyo.

721

722 5. Summary

723 The SLUCM, which has many users worldwide, has limitations including constant
724 anthropogenic heat (Q_F) and fully adiabatic conditions or energy imbalance within the urban
725 canopy layer in each time step. The present study addressed these limitations through
726 developing a new dynamic parameterisation: SLUCM+BEM. The development philosophy
727 underlying this parameterisation and its usage is summarised as follows.

728 To maintain the simplicity that is the major advantage of SLUCM, we addressed its
729 limitations as simply as possible and proposed a dynamic parameterisation of electricity
730 consumption (EC) and Q_F from buildings (Q_{FB}), designated SLUCM+BEM. To address the
731 limitations of SLUCM, the most critical process was calculating conductive heat transfer,
732 from which EC and Q_{FB} are calculated. In doing so, windows and ventilation are not
733 considered for the sake of simplicity.

734 The input parameters for BEP+BEM (HSEQUIP_SCALE_FACTOR and HSEQUIP)
735 are re-used for the calculations outlined above, and five new parameters are incorporated into
736 URBPRAM.TBL. The implementation of SLUCM+BEM is simple. Specifically, realistic
737 values are set for the new parameters, and AHOPTION is set to 2 in URBPRAM.TBL.

738 Using the proposed settings, SLUCM+BEM reproduced the radiation balance and
739 surface heat budget within the urban canopy layer at Tokyo (Yoyogi) in summer (cooling
740 season) and winter (heating season) as well as SLUCM. SLUCM+BEM reproduced the
741 temporal variation and spatial distribution of air temperature in summer (cooling season) and
742 winter (heating season) as well as SLUCM.

743 The development of SLUCM+BEM enables the dynamic calculation of EC and Q_{FB} .
744 SLUCM+BEM provided good representation of the temporal variation and spatial
745 distribution of EC_{HAC} in summer (cooling season) and winter (heating season). Compared to
746 the more sophisticated model CM-BEM, SLUCM+BEM less accurately reproduced the fine
747 spatial distribution in urban areas and error metrics, particularly in BC grids. However,
748 SLUCM+BEM showed similar accuracy to CM-BEM in reproducing spatially averaged
749 values, particularly in summer. The reproducibility of EC suggests that Q_{FB} calculated from
750 EC is also fairly realistic.

751 SLUCM+BEM introduces several processes (i.e., partial HAC, COP changes, and
752 cooling towers) that are not considered in the official BEP+BEM. Of these processes, the
753 consideration of partial HAC is most critical, as it significantly affects the value of Q_{FB} .
754 Therefore, it is essential to introduce the five new parameters as accurately as possible.

755 The source code for SLUCM+BEM has been made openly available (Takane et al.,
756 2024b); thus, it may be freely accessed by WRF and SLUCM users.

757

758 Data Availability Statement

759 All datasets analysed in this work are publicly available. The WRF model may be
760 downloaded at <https://github.com/wrf-model> (last accessed: 11/09/2023). The input data and
761 source code for WRF-SLUCM+BEM used in this study have been archived on Zenodo at
762 <https://doi.org/10.5281/zenodo.10685693> (Takane et al., 2024a) and
763 <https://doi.org/10.5281/zenodo.10686465> (Takane et al., 2024b), respectively.

764

765 Acknowledgements

766 This study was supported by the Environmental Research and Technology
767 Development Fund (grant no. JPMEERF20231007) of the Environmental Restoration and
768 Conservation Agency of Japan. We were also supported by a Japan Society for the Promotion
769 of Science (JSPS) KAKENHI grant (no. JP23H01544). The calculations were performed
770 using the supercomputer system (NEC SX-Aurora TSUBASA) of the National Institute for
771 Environmental Studies. We thank Dr. Masayuki Hara of the Japan Meteorological Agency for
772 his technical support using the LULC datasets of the Geospatial Information Authority of
773 Japan for WRF simulations.

774

775 **References**

- 776 Adachi, S. A., Kimura, F., Kusaka, H., Duda, M. G., Yamagata, Y., Seya, H., Nakamichi, K., &
777 Aoyagi, T. (2014), Moderation of summertime heat island phenomena via modification of the
778 urban form in the Tokyo metropolitan area. *Journal of Applied Meteorology and Climatology*,
779 53(8), 1886–1900. doi: 10.1175/JAMC-D-13-0194.1
- 780 Bäumer, D., & Vogel, B. (2007), An unexpected pattern of distinct weekly periodicities in
781 climatological variables in Germany. *Geophysical Research. Letters*, 34, L03819. doi:
782 10.1029/2006GL028559
- 783 Bueno, B., Pigeon, G., Norford, L. K., Zibouche, K., & Marchadier, C. (2012), Development and
784 evaluation of a building energy model integrated in the TEB scheme. *Geoscientific Model
785 Development*, 5(2), 433–448. doi:10.5194/gmd-5-433-2012
- 786 Chao, Y., Li, Z., Farrara, J. D., & Hung, P. (2009), Blending sea surface temperatures from multiple
787 satellites and in situ observations for coastal oceans. *Journal of Atmospheric and Oceanic
788 Technology*, 26(7), 1415–1426. doi:10.1175/2009JTECHO592.1
- 789 Chen, F., & Dudhia, J. (2001), Coupling and advanced land surface-hydrology model with the Penn
790 State-NCAR MM5 modeling system. Part I: Model implementation and sensitivity. *Monthly
791 Weather Review*, 129(4), 569–585. doi:10.1175/1520-0493(2001)129<0569:CAALSH>2.0.CO;2
- 792 Chen, F., Kusaka, H., Bornstein, R., Ching, J., Grimmond, C. S. B., Grossman-Clarke, S., Loridan, T.,
793 Manning, K. W., Martilli, A., Miao, S., Sailor, D., Salamanca, F., P., Taha, H., Tewari, M.,
794 Wang, X., Wyszogrodzki, A. A., & Zhang, C. (2011), The integrated WRF/urban modelling
795 system: development, evaluation, and applications to urban environmental problems.
796 *International Journal of Climatology*, 31(2), 273–288. doi:10.1002/joc.2158
- 797 Chen, L., X. Zheng, J. Yang., & J. H. Yoon. (2021), Impact of BIPV windows on building energy
798 consumption in street canyons: Model development and validation. *Energy and Buildings*, 249,
799 11207. doi:10.1016/j.enbuild.2021.111207
- 800 Demuzere, M., Kittner, J., Martilli, A., Mills, G., Moede, C., Stewart, I. D., van Vliet, J., & Bechtel, B.
801 (2022), A global map of local climate zones to support earth system modelling and urban-scale
802 environmental science, *Earth System. Science Data*, 14, 3835–3873. doi:10.5194/essd-14-3835-
803 2022
- 804 Doan, V. Q., Kusaka, H., & Nguyen, T. M. (2019), Roles of past, present, and future land use and
805 anthropogenic heat release changes on urban heat island effects in Hanoi, Vietnam: Numerical
806 experiments with a regional climate model. *Sustainable Cities and Society*, 47, 101479.
807 doi:10.1016/j.scs.2019.101479
- 808 Earl, N., Simmonds, I. & Tappe, N. (2016), Weekly cycles in peak time temperatures and urban heat
809 island intensity. *Environental Research Letters*, 11, 074003. doi:10.1088/1748-9326/11/7/074003
- 810 Fujibe, F. (1987), Weekday-weekend differences of urban climates Part 1: temporal variation of air
811 temperature. *Journal of Meteorological Society of Japan*, 65, 923–929.
812 doi:10.2151/jmsj1965.65.6_923
- 813 Fujibe, F. (2010), Day-of-the-week variations of urban temperature and their long-term trends in
814 Japan. *Theor. Appl. Climatol.* 104, 393–401. doi:10.1007/s00704-010-0266-y
- 815 Gamarro, H. & González-Cruz, J. E. (2023), On the electrification of winter season in cold climate
816 megacities—The case of New York City. *J. Eng. Sustain. Bldgs. Cities*, 4(3), 031006.
817 doi:10.1115/1.4063377
- 818 GDAS, N. (2015), FNL 0.25 Degree Global Tropospheric Analyses and Forecast Grids. Research
819 Data Archive at the National Center for Atmospheric Research; Computational and Information
820 Systems Laboratory: Boulder, CO, USA.
- 821 Georgescu, M., Morefield, P. E., Bierwagen, B. G. & Weaver, C. P., (2014), Urban adaptation can roll
822 back warming of emerging megapolitan regions. *Proc. Natl. Acad. Sci.*, 111, 2909–2914.
823 doi:10.1073/pnas.1322280111
- 824 Grimmond, C. S. B., Blackett, M., Best, M. J., Barlow, J., Baik, J.-J., Belcher, S. E., Bohnenstengel, S.
825 I., Calmet, I., Chen, F., Dandou, A., Fortuniak, K., Gouvea, M. L., Hamdi, R., Hendry, M.,
826 Kawai, T., Kawamoto, Y., Kondo, H., Krayenhoff, E. S., Lee, S.-H., Loridan, T., Martilli, A.,
827 Masson, V., Miao, S., Olsen, K., Pigeon, G., Porson, A., Ryu, Y.-H., Salamanca, F., Shashua-

828 Bar, L., Steeneveld, G.-J., Tombrou, M., Voogt, J., Young, D., & Zhang, N. (2010), The
829 international urban energy balance models comparison project: first results from phase 1.
830 *Journal of Applied Meteorology and Climatology*, 49, 1268–1292. doi:10.1175/2010JAMC2354.1.
831 Grimmond, C. S.B., Blackett, M., Best, M. J., Baik, J.-J., Belcher, S. E., Beringer, J., Bohnenstengel,
832 S. I., Calmet, I., Chen, F., Coutts, A., Dandou Fortuniak, K., Gouvea, M. L., Hamdi, R., Hendry,
833 M., Kanda, M., Kawai, T., Kawamoto, Y., Kondo, H., Krayenhoff, E. S., Lee, S.-H., Loridan, T.,
834 Martilli, A., Masson, V., Miao, S., Olsen, K., Ooka, R., Pigeon, G., Porson, A., Ryu, Y.-H.,
835 Salamanca, F., Steeneveld, G. J., Tombrou, M., Voogt, J., Young, D., & Zhang, N. (2011), Initial
836 results from phase 2 of the International Urban Energy Balance Model Comparison.
837 *International Journal of Climatology*, 31, 244–272, doi:10.1002/joc.2227.
838 Hirsch, A. L., Evans, J. P., Thomas, C., Conroy, B., Hart, M. A., Lipson, M., & Ertler, W. (2021),
839 Resolving the influence of local flows on urban heat amplification during heatwaves.
840 *Environmental Research Letters*, 16, 064066. doi: 10.1088/1748-9326/ac0377
841 Hirano, T., Sugawara, H., Murayama, S. & Kondo, H. (2015), Diurnal variation of CO₂ flux in an
842 urban area of Tokyo. *Scientific Online Letters On The Atmosphere*, 11, 100–103.
843 doi:10.2151/sola.2015-024
844 Iacono, M. J., Delamere, J. S., Mlawer, E. J., Shephard, M. W., Clough, S. A., & Collins, W. D.
845 (2008), Radiative forcing by long-lived greenhouse gases: Calculations with the AER radiative
846 transfer models. *Journal of Geophysical Research – Atmosphere*, 113, D13103.
847 doi:10.1029/2008JD009944
848 IEA. (2018). The Future of Cooling. <https://www.iea.org/reports/the-future-of-cooling>
849 Ihara, T., Kikegawa, Y., Asahi, K., Genchi, Y., & Kondo, H. (2008), Changes in year-round air
850 temperature and annual energy consumption in office building areas by urban heat-island
851 countermeasures and energy-saving measures. *Applied Energy*, 85(1), 12–25.
852 doi:10.1016/j.apenergy.2007.06.012
853 Janjic, Z. I. (1994), The Step-Mountain Eta Coordinate Model: Further Developments of the
854 Convection, Viscous Sublayer, and Turbulence Closure Schemes. *Monthly Weather Review*,
855 122(5), 927–945. [https://doi.org/10.1175/1520-0493\(1994\)122<0927:TSMECM>2.0.CO;2](https://doi.org/10.1175/1520-0493(1994)122<0927:TSMECM>2.0.CO;2)
856 Janjic, Z. I. (2001), Nonsingular Implementation of the Mellor-Yamada Level 2.5 Scheme in the
857 NCEP Meso model, National Centers for Environmental Prediction, Office Note #437,
858 (February), 1–61.
859 Järvi, L., Grimmond, C. S. B., & Christen, A. (2011), The surface urban energy and water balance
860 scheme (SUEWS): evaluation in Los Angeles and Vancouver. *Journal of Hydrology*, 411 (3–4),
861 219-237. doi:10.1016/j.jhydrol.2011.10.001
862 Järvi, L., Grimmond, C. S. B. Taka, M., Nordbo, A., Setälä, H., & Strachan, I. B. (2014),
863 Development of the Surface Urban Energy and Water Balance Scheme (SUEWS) for cold
864 climate cities, *Geoscientific Model Development*, 7(4), 1691–1711. doi:10.5194/gmd-7-1691-
865 2014
866 Khanh, D. N., Varquez, A. C. G., & Kanda, M. (2023), Impact of urbanization on exposure to extreme
867 warming in megacities. *Heliyon*, 9, e1551. doi:10.1016/j.heliyon.2023.e15511
868 Kikegawa, Y., Genchi, Y., Yoshikado, H., & Kondo, H. (2003), Development of a numerical
869 simulation system toward comprehensive assessments of urban warming countermeasures
870 including their impacts upon the urban buildings' energy-demands. *Applied Energy*, 76(4), 449–
871 466. doi:10.1016/S0306-2619(03)00009-6
872 Kikegawa Y, Genchi Y, Kondo H. Impacts of the component patterns of air conditioning system and
873 power supply system in buildings upon urban thermal environment in summer. *Environ Syst Res*
874 2005;33:189–97. doi:10.2208/proer.33.189. in Japanese with English abstract.
875 Kikegawa, Y., Tanaka, A., Ohashi, Y., Ihara, T., & Shiget, Y. (2014), Observed and simulated
876 sensitivities of summertime urban surface air temperatures to anthropogenic heat in downtown
877 areas of two Japanese Major Cities, Tokyo and Osaka. *Theoretical and Applied Climatology*,
878 117(1), 175–193. doi:10.1007/s00704-013-0996-8
879 Kikegawa, Y., Nakajima, K., Takane, Y., Ohashi, Y., & Ihara, T. (2022), A quantification of classic
880 but unquantified positive feedback effects in the urban-building-energy-climate system. *Applied*
881 *Energy*, 307, 118227. doi:10.1016/j.apenergy.2021.118227
882 Krayenhoff, E. S., Broadbent, A.M., Zhao, L., Georgescu, M., Middel, A., Voogt, J.A., Martilli, A.,

883 Sailor, D.J., & Erell, E. (2021), Cooling hot cities: a systematic and critical review of the
884 numerical modelling literature. *Environmental Research Letters*, 16, 053007. doi:10.1088/1748-
885 9326/abdcf1

886 Krayenhoff, E. S., Moustaoi, M., Broadbent, A. M., Gupta, V. & Georgescu, M. (2018), Diurnal
887 interaction between urban expansion, climate change and adaptation in US cities. *Nature Climate*
888 *Change*, 8, 1097–1103. doi:10.1038/s41558-018-0320-9

889 Kusaka, H., Hara, M., & Takane, Y. (2012), Urban climate projection by the WRF model at 3-km grid
890 increment: Dynamical downscaling and predicting heat stress in the 2070's August for Tokyo,
891 Osaka, and Nagoya metropolises. *Journal of the Meteorological Society of Japan*, 90B, 47-64.
892 doi:10.2151/jmsj.2012-B04

893 Kusaka, H., & Kimura, F. (2004), Coupling a Single-Layer Urban Canopy Model with a Simple
894 Atmospheric Model: Impact on Urban Heat Island Simulation for an Idealized Case. *Journal of*
895 *the Meteorological Society of Japan*, 82(1), 67–80. doi:10.2151/jmsj.82.67

896 Kusaka, H., Kondo, H., Kikegawa, Y., & Kimura, F. (2001), A Simple Single-Layer Urban Canopy
897 Model for Atmospheric Models: Comparison with Multi-Layer and Slab Models. *Boundary-*
898 *Layer Meteorology*, 101(ii), 329–358. doi:10.1023/A:1019207923078

899 Kusaka, H., Nawata, K., Suzuki-Parker, A., Takane, Y. & Furuhashi, N. (2014), Mechanism of
900 precipitation increase with urbanization in Tokyo as revealed by ensemble climate simulations.
901 *Journal of Applied Meteorology and Climatology*, 53, 824–839. doi:10.1175/JAMC-D-13-065.1

902 Miao, S., Chen, F., LeMone, M. A., Tewari, M., Li, Q. & Wang, Y. (2009), An observational and
903 modeling study of characteristics of urban heat island and boundary layer structures in Beijing.
904 *Journal of Applied Meteorology and Climatology*, 48, 484–501. doi:10.1175/2008JAMC1909.1

905 Lipson, M., Grimmond, C. S. B., Best, M., Abramowitz, G., Coutts, A., Tapper, N., Baik, J.-J., Beyers,
906 M., Blunn, L., Boussetta, S., Bou-Zeid, E., De Kauwe, M. G., de Munck, C., Demuzere, M.,
907 Faticchi, S., Fortuniak, K., Han, B.-S., Hendry, M., Kikegawa, Y., Kondo, H., Lee, D.-Il, Lee, S.-
908 H., Lemonsu, A., Machado, T., Manoli, G., Martilli, A., Masson, V., McNorton, J., Meili, N.,
909 Meyer, D., Nice, K. A., Oleson, K. W., Park, S.-B., Roth, M., Schoetter, R., Simón-Moral, A.,
910 Steeneveld, G.-J., Sun, T. Takane, Y., Thatcher, M., Tsiringakis, A., Varentsov, M., Wang, C.,
911 Wang, Z.-H., & Pitman, A. (2023), Evaluation of 30 urban land surface models in the Urban-
912 PLUMBER project: Phase 1 results. *Quarterly Journal of the Royal Meteorological Society*, in
913 press. doi:10.1002/qj.4589

914 Lipson, M., Grimmond, S., Best, M., Chow, W.T.L., Christen, A., Chrysoulakis, N. et al. (2022),
915 Harmonized gap-filled datasets from 20 urban flux tower sites. *Earth System Science Data*, 14,
916 5157–5178. doi:10.5194/essd-14-5157-2022

917 Lipson, M. J., Thatcher, M., Hart, M. A., & Pitman, A. (2018), A building energy demand and urban
918 land surface model. *Quarterly Journal of the Royal Meteorological Society*, 144(714), 1572–
919 1590. doi:10.1002/qj.3317

920 Loridan, T., Grimmond, C. S. B., Grossman-Clarke, S., Chen, F., Tewari, M., Manning, K., Martilli,
921 A., Kusaka, H., & Best, M. (2010), Trade-offs and responsiveness of the single-layer urban
922 canopy parametrization in WRF: An offline evaluation using the MOSCEM optimization
923 algorithm and field observations. *Quarterly Journal of the Royal Meteorological Society*,
924 136(649), 997–1019. doi:10.1002/qj.614

925 Martilli, A., Clappier, A., & Rotach, M. W. (2002), An urban surface exchange parameterization for
926 mesoscale models. *Boundary-Layer Meteorology*, 104, 261–304, doi:10.1023/A:1016099921195

927 Mellor, G. L., & Yamada, T. (1982), Development of a Turbulence Closure Model for Geophysical
928 Fluids Problems. *Reviews of Geophysics and Space Physics*, 20(4), 851–875.
929 doi:10.1029/RG020i004p00851

930 Morrison, H., Thompson, G., & Tatarskii, V. (2009), Impact of cloud microphysics on the
931 development of trailing stratiform precipitation in a simulated squall line: Comparison of one-
932 and two-moment schemes. *Monthly Weather Review*, 137(3), 991–1077.
933 doi:10.1175/2008MWR2556.1

934 Nakajima, K., Takane, Y., Fukuba, S., Yamaguchi, K., & Kikegawa, Y. (2022), Urban electricity–
935 temperature relationships in the Tokyo Metropolitan Area. *Energy and Buildings*, 256, 111729.
936 doi:10.1016/j.enbuild.2021.111729

937 Nakajima, K., Takane, Y., Kikegawa, Y., Furuta, Y., & Takamatsu, H. (2021), Human behaviour

938 change and its impact on urban climate: Restrictions with the G20 Osaka Summit and COVID-
939 19 outbreak. *Urban Climate*, 35, 100728. doi:10.1016/j.uclim.2020.100728

940 Nakajima, K., Takane, Y., Kikegawa, Y. & Yamaguchi, K. (2023), Improvement of WRF–CM–BEM
941 and its application to high-resolution hindcasting of summertime urban electricity consumption.
942 *Energy and Buildings*, 296, 113336. doi:10.1016/j.enbuild.2023.113336

943 NCEP (2015). National Centers for Environmental Prediction/National Weather Service/NOAA/U.S.
944 Department of Commerce. NCEP GDAS/FNL 0.25 Degree global tropospheric analyses and
945 forecast grids; 2015. <https://doi.org/10.5065/D65Q4T4Z>.

946 Ohashi, Y., Genchi, Y., Kondo, H., Kikegawa, Y., Yoshikado, H., & Hirano, Y. (2007), Influence of
947 air-conditioning waste heat on air temperature in Tokyo during summer: Numerical experiments
948 using an urban canopy model coupled with a building energy model. *Journal of Applied
949 Meteorology and Climatology*, 46(1), 66–81. doi:10.1175/JAM2441.1

950 Ohashi, Y., Suido, M., Kikegawa, Y., Ihara, T., Shigeta, Y. & Nabeshima, M. (2016), Impact of
951 seasonal variations in weekday electricity use on urban air temperature observed in Osaka, Japan.
952 *Quarterly Journal of Meteorological Society*, 142, 971–982. doi: 10.1002/qj.2698

953 Oleson, K. W., Bonan, G. B., Feddema, J., Vertenstein, M., & Grimmond, C. S. B. (2008), An urban
954 parameterization for a global climate model. Part I: Formulation and evaluation for two cities.
955 *Journal of Applied Meteorology and Climatology*, 47(4), 1038–1060.
956 doi:10.1175/2007JAMC1597.1

957 Oleson, K. W., & Feddema, J. (2020), Parameterization and surface data improvements and new
958 capabilities for the Community Land Model Urban (CLMU). *Journal of Advances in Modeling
959 Earth Systems*, 12(2), e2018MS001586. doi:10.1029/2018MS001586

960 Salamanca, F., Krpo, A., Martilli, A., & Clappier, A. (2010), A new building energy model coupled
961 with an urban canopy parameterization for urban climate simulations—part I. formulation,
962 verification, and sensitivity analysis of the model. *Theoretical and Applied Climatology*, 99(3–4),
963 331–344. doi:10.1007/s00704-009-0142-9

964 Salamanca, F., Georgescu, M., Mahalov, A., Moustauoui, M., Wang, M., & Svoma, B. M. (2013),
965 Assessing summertime urban air conditioning consumption in a semiarid environment.
966 *Environmental Research Letters*, 8(3), 034022. doi:10.1088/1748-9326/8/3/034022

967 Salamanca, F., Georgescu, M., Mahalov, A., Moustauoui, M., & Wang, M. (2014), Anthropogenic
968 heating of the urban environment due to air conditioning. *Journal of Geophysical Research:
969 Atmospheres*, 119(10), 5949–5965. doi:10.1002/2013JD021225

970 Skamarock, W. C., Klemp, J. B., Dudhia, J., Gill, D. O., Liu, Z., Berner, J., ... Huang, X. -yu. (2021).
971 A Description of the Advanced Research WRF Model Version 4.3 (No. NCAR/TN-556+STR).
972 doi:10.5065/1dfh-6p97

973 Sugawara, H., Ishidoya, S., Terao, Y., Takane, T., Kikegawa, Y., & Nakajima, K. (2021),
974 Anthropogenic CO₂ emissions changes in an urban area of Tokyo, Japan due to the COVID-19
975 pandemic: A case study during the state of emergency in April-May 2020. *Geophysical Research
976 Letters*, 48, e2021GL092600. doi:10.1029/2021GL092600

977 Sun, T., Omidvar, H., Li, Z., Zhang, N., Huang, W., Kotthaus, S., Ward, H. C., Luo, Z., & Grimmond,
978 S. (2024), WRF (v4.0)–SUEWS (v2018c) coupled system: development, evaluation and
979 application, *Geoscientific Model Development*, 17, 91–116. doi:10.5194/gmd-17-91-2024.

980 Takane, Y., Kikegawa, Y., Hara, M., Ihara, T., Ohashi, Y., Adachi, S. A., et al. (2017), A
981 climatological validation of urban air temperature and electricity demand simulated by a regional
982 climate model coupled with an urban canopy model and a building energy model in an Asian
983 megacity. *International Journal of Climatology*, 37(1), 1035–1052. doi:10.1002/joc.5056

984 Takane, Y., Kikegawa, Y., Hara, M., & Grimmond, C. S. B. (2019), Urban warming and future air-
985 conditioning use in an Asian megacity : importance of positive feedback. *NPJ Climate and
986 Atmospheric Science*, 2, 39. doi:10.1038/s41612-019-0096-2

987 Takane, Y., Kikegawa, Y., Nakajima, K., & Kusaka, H. (2024a), WRF–SLUCM+BEM: Input data for
988 the evaluation at Tokyo Metropolitan Area. Zendo [data set]. doi:10.5281/zenodo.10685693

989 Takane, Y., Kikegawa, Y., Nakajima, K., & Kusaka, H. (2024b), WRF–SLUCM+BEM source code
990 for JAMES submission. Zendo [code]. doi:10.5281/zenodo.10686465

991 Takane, Y. & Kusaka, H. (2011), Formation mechanisms of the extreme high surface air temperature
992 of 40.9°C observed in the Tokyo metropolitan area: Considerations of dynamic foehn and

993 foehnlike wind. *Journal of Applied Meteorology and Climatology*, 50, 1827-1841. doi:
994 10.1175/JAMC-D-10-05032.1

995 Takane, Y., Ohashi, Y., Grimmond, C. S. B., Hara, M., & Kikegawa, Y. (2020), Asian megacity heat
996 stress under future climate scenarios: impact of air-conditioning feedback. *Environmental*
997 *Research Communications*, 2, 015004. doi:10.1088/2515-7620/ab6933

998 Takane, Y., Nakajima, K., & Kikegawa, Y. (2022), Urban climate changes during the COVID-19
999 pandemic: integration of urban-building-energy model with social big data. *NPJ Climate and*
1000 *Atmospheric Science*, 5, 44. doi:10.1038/s41612-022-00268-0

1001 Takane, Y., Nakajima, K., Kikegawa, Y. & Yamaguchi, K. (2023b), Enhancing urban canopy building
1002 energy models through the integration of social big data: Improvement and application,
1003 *International Association for Urban Climate (IAUC) Urban Climate News*, 89, 17-21.

1004 Takane, Y., Nakajima, K., Yamaguchi, K., & Kikegawa, Y. (2023a), Decarbonisation technologies
1005 can halve the nonlinear increase in electricity demand in densely populated areas due to climate
1006 change. *Sustainable Cities and Society*, 99, 104966. doi:10.1016/j.scs.2023.104966

1007 Tsiringakis, A., Steeneveld, G.-J. Holtslag, A. A. M., Kotthaus, S., & Grimmond, C. S. B. (2019), On-
1008 and off-line evaluation of the single-layer urban canopy model in London summertime
1009 conditions. *Quarterly Journal of the Royal Meteorological Society*, 145(721), 1474–1489.
1010 doi:10.1002/qj.3505

1011 Umezaki, A. S., Ribeiro, F. N. D., de Oliveira, A. P., Soares, J., & de Miranda, R. M. (2020),
1012 Numerical characterization of spatial and temporal evolution of summer urban heat island
1013 intensity in São Paulo, Brazil. *Urban Climate*, 32, 100615. doi:10.1016/j.uclim.2020.100615

1014 Varquez, A. C. G., Kiyomoto, S., Khanh, D. N. & Kanda. M. (2021), Global 1-km present and future
1015 hourly anthropogenic heat flux. *Scientific Data*, 8, 64. doi:10.1038/s41597-021-00850-w

1016 Wang, C., Wang, Z.-H., & Ryu, Y.-H. (2021), A single-layer urban canopy model with transmissive
1017 radiation exchange between trees and street canyons, *Building and Environment*, 191, 107593.
1018 doi:10.1016/j.buildenv.2021.107593

1019 Wang, Z., Bou-Zeid, E., & Smith, J.A. (2013), A coupled energy transport and hydrological model for
1020 urban canopies evaluated using a wireless sensor network. *Q. J. R. Meteorolog. Soc.*, 139 (675),
1021 1643–1657. doi:10.1002/qj.2032

1022 Ward, H.C., Kotthaus, S., Järvi, L., & Grimmond, C.S.B. (2016), Surface Urban Energy and Water
1023 Balance Scheme (SUEWS): Development and evaluation at two UK sites. *Urban Climate*, 18, 1–
1024 32. doi:10.1016/j.uclim.2016.05.001

1025 Xu, X., Chen, F., Shen, S., Miao, S., Barlage, M., Guo, W., & Mahalov, A. (2018), Using WRF-Urban
1026 to assess summertime air conditioning electric loads and their impacts on urban weather in
1027 Beijing. *Journal of Geophysical Research: Atmospheres*, 123(5), 2475–2490.
1028 doi:10.1002/2017JD028168

1029 Yamazaki, M., Egusa, T., Shimoda, Y., & Mizuno, M. (2002), Study on energy consumption
1030 characteristics of small scale building with unit air conditioner. *Transactions of the Society of*
1031 *Heating, Air-conditioning and Sanitary Engineers of Japan*, 27, 15–23. (in Japanese with
1032 English abstract). doi:10.18948/shase.27.84_15

1033 Yu, M., González, J., Miao, S., & Ramamurthy, P. (2019), On the assessment of a cooling tower
1034 scheme for high-resolution numerical weather modeling for urban areas. *Journal of Applied*
1035 *Meteorology and Climatology*, 58(6), 1399–1415. doi:10.1175/JAMC-D-18-0126.1

1036